



Study of acoustic transmission losses in particle-reinforced rubber-based membrane-type acoustic metamaterials



Junyu Li, Renjie Jiang, Di Xu, Qibai Huang*

State Key Laboratory of Digital Manufacturing Equipment and Technology, School of Mechanical Science and Engineering, Huazhong University of Science and Technology, Wuhan, China

ARTICLE INFO

Article history:

Received 25 November 2022

Received in revised form 26 February 2023

Accepted 7 April 2023

Available online 11 April 2023

Keywords:

Particle reinforcement

EPDM/ETFE

Molecular dynamics

Mechanical properties

Sound transmission loss

ABSTRACT

In this work, the mechanical properties of particle reinforced ethylene propylene diene monomer (EPDM)/ethylene tetrafluoroethylene (ETFE) copolymer material were determined by molecular dynamics (MD) method, and the copolymer material was used in the structural design of acoustic metamaterials. Secondly, based on the discrete point matching method, the acoustic transmission loss characteristics of the material are predicted, and the accuracy and effectiveness of the theory are verified through the multi physical field coupling finite element model. Finally, seven key parameters that affect the material structure are studied, and their influencing rules and mechanisms are analyzed. The results show that the structure makes up for the sound insulation defect of traditional ETFE film materials at low frequencies. Through reasonable selection of key parameters, high sound insulation design can be carried out for specific frequency bands, which is of great significance to the potential application in the construction field (new building materials).

© 2023 Elsevier Ltd. All rights reserved.

1. Introduction

ETFE has received a great deal of current interest due to its excellent thermal, electrical and optical properties [1,2]. This polymer material has the common advantages of ethylene and tetrafluoroethylene and exhibits macroscopic properties such as lightness, transparency and durability, and is considered by the construction industry as an alternative to glass [3]. ETFE polymer films can be flexibly composed in single or multiple layers, in line with the general characteristics of high-performance materials for construction [4,5]. The weight of a single layer of ETFE film and ETFE cushion is approximately 1% of that of glass, which is extremely light and can significantly reduce the load on the structural frame. At the same time, the ability of ETFE polymer films to replace glass in older structures to meet current building codes has significant cost advantages. The researchers conducted in-depth exploration on the mechanical properties [6–10], light transmission [11–15], service life [16–19], energy conservation and emission reduction [20–22] of ETFE. In addition, ETFE membrane materials have been widely used in the construction industry, including the Arnhem Burger Botanical Garden in the Netherlands in 1982 [23,24], the National Stadium “Bird’s Nest” and the National Swimming Center

“Water Cube” in the 2008 Beijing Olympic Games [25], the British National Space Center and the Belgian Transparent Church.

However, the acoustic properties of ETFE are particularly important as a long-term construction material. Although ETFE polymer films are UV resistant, highly reflective, waterproof and dustproof, their acoustic properties are not as good as they could be due to their thinness and light weight [26,27]. The conventional methods of improving its acoustic performance are still focused on combining it with a certain quality of rigid material [28,29]. This method increases the thickness and mass of the structure to a certain extent, and it improves the sound insulation performance in the middle and high frequency range, while the low frequency sound insulation is still not properly dealt with.

EPDM is one of the best acoustic rubbers available [30], with high mechanical strength and dimensional stability over a wide temperature range (especially at high temperatures) [31]. Therefore, compounding EPDM with other polymers has become an effective means of improving the acoustic properties of polymeric materials [32]. Some researchers have compounded EPDM with PP to produce a polymer material with good sound insulation properties in the range of 3000 Hz–6000 Hz [33–35]. In addition, some researchers have also formed a composite material from polyurethane (PU) and EPDM, which effectively improved the average sound absorption coefficient of the material [36]. In this paper,

* Corresponding author.

E-mail address: qbhuang@hust.edu.cn (Q. Huang).



ScienceDirect 提供的目录列表可用

应用声学

期刊主页: www.elsevier.com/locate/apacoust



颗粒增强橡胶基膜型声学超材料中声传输损失的研究



李俊宇, 姜仁杰, 徐迪, 黄启白

华中科技大学机械科学与工程学院数字制造装备与技术国家重点实验室, 中国湖北武汉

一篇文章 i n f o

文章历史:

2022 年 11 月 25 日收到 2023 年 2 月 26 日
修订后接受 2023 年 4 月 7 日接受 在线可用
2023 年 4 月 11 日

关键词:

粒子增强 EPDM/ETFE 分子
动力学 机械性能 声传输损
失

摘要

在这项工作中, 通过分子动力学 (MD) 方法确定了颗粒增强乙烯丙烯橡胶 (EPDM) / 四氟乙烯 (ETFE) 共聚物材料的力学性能, 并将共聚物材料用于声学超材料的结构设计。其次, 基于离散点匹配方法, 预测了材料的声学传输损耗特性, 并通过多物理场耦合有限元模型验证了理论的准确性和有效性。最后, 研究了影响材料结构的七个关键参数, 分析了它们的影响规律和机制。结果表明, 该结构弥补了传统 ETFE 薄膜材料在低频时的隔音缺陷。通过合理选择关键参数, 可以针对特定频段进行高隔音设计, 对潜在应用于建筑领域 (新建筑材料) 具有重要意义。

2023 Elsevier Ltd. 版权所有。保留所有权利。

1. 简介 ETFE 由于其出色的热学、电学和光学性能而受到了广泛关注 [1,2]。这种聚合物材料具有乙烯和四氟乙烯的共同优点, 并表现出轻盈、透明和耐用等宏观特性, 被建筑行业视为玻璃的替代品[3]。ETFE 聚合物薄膜可以灵活地组成单层或多层, 符合建筑高性能材料的一般特性[4,5]。单层 ETFE 薄膜和 ETFE 气垫的重量约为玻璃的 1%, 极为轻盈, 可以显著减轻结构框架的负荷。同时, ETFE 聚合物薄膜能够替代老建筑中的玻璃以符合当前建筑法规, 具有显著的成本优势。研究人员对 ETFE 的机械性能[6–10]、光传输[11–15]、使用寿命[16–19]、节能减排[20–22]等进行了深入探讨。此外, ETFE 膜材料已广泛应用于建筑行业, 包括 1982 年在荷兰阿纳姆的博格植物园

2008 年北京奥运会的国家体育场“鸟巢”和国家游泳中心“水立方”, 英国国家太空中心和比利时透明教堂。

然而, ETFE 的声学特性在作为长期建筑材料时尤为重要。尽管 ETFE 聚合物薄膜具有抗紫外线、高反射、防水和防尘的特性, 但由于其薄和轻的特点, 其声学性能并不尽如人意。目前改善其声学性能的传统方法仍然集中在将其与一定质量的刚性材料结合。这种方法在一定程度上增加了结构的厚度和质量, 并提高了中高频范围的隔音性能, 但低频隔音仍未得到妥善处理。

EPDM 是目前最好的声学橡胶之一[30], 具有高机械强度和在宽温度范围内的尺寸稳定性 (尤其是在高温下) [31]。因此, 将 EPDM 与其他聚合物混合已成为改善聚合材料声学性能的有效手段[32]。一些研究人员已将 EPDM 与 PP 混合, 以生产在 3000 Hz–6000 Hz 范围内具有良好隔音性能的聚合物材料[33–35]。此外, 一些研究员还将聚氨酯 (PU) 和 EPDM 形成复合材料, 有效提高了材料的平均吸声系数[36]。在本文中,

† 通讯作者。

电子邮件地址: qbhuang@hust.edu.cn (Q. Huang)。

we chose to composite EPDM with ETFE to improve the acoustic properties of polymer materials.

Carbon nanostructures such as single-layer carbon nanotubes, double-layer carbon nanotubes and carbon nanoparticles have received great attention in the past decades because of their strong mechanical properties that can be used as enhancers of the mechanical properties of the matrix material [37–39]. Whereas the mechanical properties of EPDM are lower than those of ETFE, by introducing carbon nanostructures, the EPDM/ETFE materials can be used to enhance the macroscopic properties.

In order to study the mechanical properties of such particle-reinforced composite polymer materials, molecular dynamics (MD) is considered a very useful analytical method [40], which can greatly reduce the required workload from the design stage of the material and calculate the mechanical properties between the polymer and the nano-filled material well [41,42], and obtain accurate macroscopic mechanical properties for the study of its acoustic properties provide the necessary data support.

Membrane-type acoustic metamaterials (MAMs) are a type of structure that can target a specific frequency range for effective sound insulation [43]: by design, targeting frequency bands can occur in the low frequency range. Therefore, the structural design of MAMs has been studied intensively and extensively by researchers. However, theoretical studies on the sound transmission losses of MAMs are still scarce: the literature [44] investigated the effect of mass blocks on the sound transmission losses of MAMs; Langfeldt et al. [45] introduced a method based on the grid convergence index to speed up the calculation of sound transmission losses.

In this study, EPDM, ETFE and carbon nanostructures were compounded for the first time, and such particle-reinforced polymer films were designed as MAMs structures to investigate their mechanical and acoustic properties. Therefore, this work firstly uses the MD method to calculate the mechanical properties of particle-reinforced EPDM/ETFE films. Secondly, a prediction model for the sound transmission loss of this thin film metamaterial is constructed based on the discrete point matching method. At the same time, the FE model of acoustic-structural coupling is developed by COMSOL Multiphysics software to verify the accuracy of the theoretical part. Finally, the sound insulation effect of particle-reinforced EPDM/ETFE thin-film acoustic metamaterials is verified by comparing polymer films and metal films of equal mass. At the same time, 7 kinds of material and structural parameters including those at different levels of the micro-macroscopic are discussed and their influence laws on the sound transmission losses are analysed.

2. Molecular dynamics calculation

2.1. Full atom model construction

EPDM is widely used in the design of sound absorbing/insulating materials because of its excellent acoustic properties. Therefore, in this study, EPDM and ETFE were selected to construct a thermoplastic material to improve the acoustic properties of the material, and then carbon nanoparticles were used to further enhance the mechanical properties of the material to improve the sound insulation effect of the composite. This material is modeled by the platform provided by BIOVIA Materials Studio 2020, and its molecular formula is shown in Fig. 1.

Firstly, an ETFE molecular chain consisting of 50 tetrafluoroethylene and an ethylene propylene diene terpolymer molecular chain consisting of ethylene, propylene, ethylidene norbornene at 70 wt%, 25 wt% and 5 wt% were established. Then, these polymers are loaded into the periodic simulation box as shown in Fig. 2 according to the component ratio of EPDM: ETFE = 3:7, and the

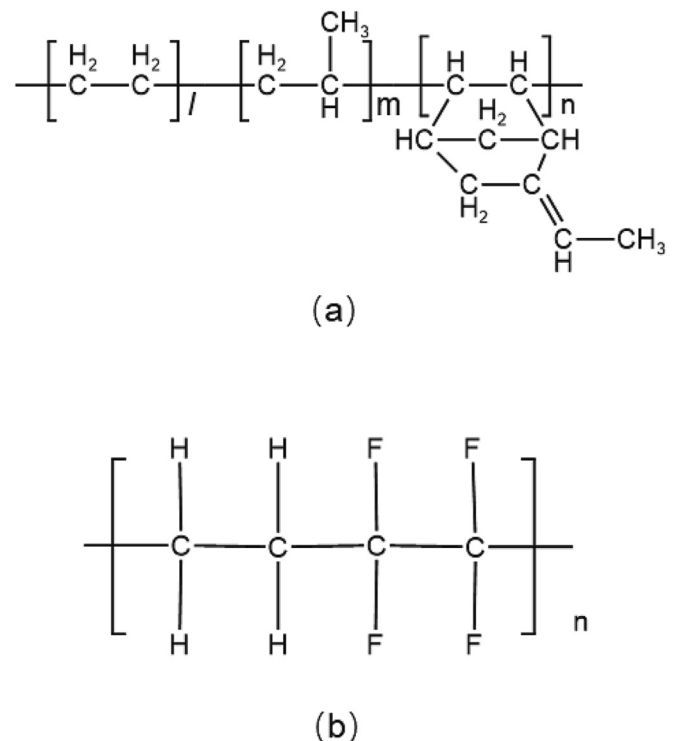


Fig. 1. Molecular Structure Formula of EPDM (a) and ETFE (b).

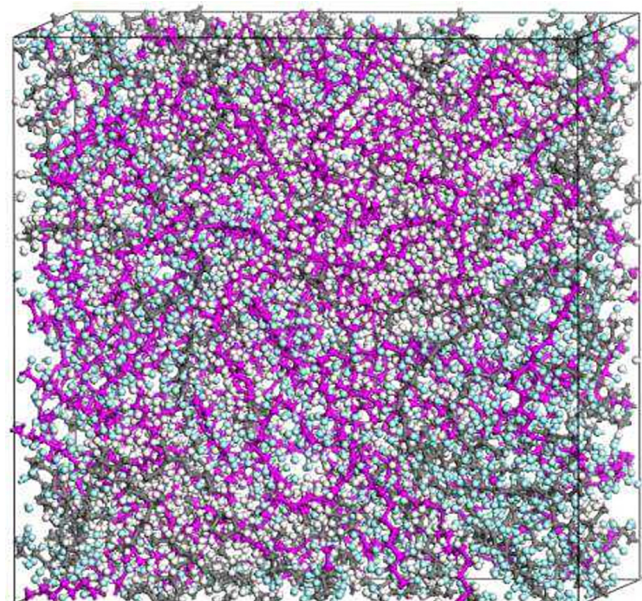


Fig. 2. Molecular Model of EPDM/ETFE Blends.

Force module in Materials Studio 2020 software is used for geometric structure optimization to obtain a reasonable three-dimensional molecular configuration. In this module, smart method is used for structural optimization. During the construction of the composite, the Amorphous Cell module in the software was used, and the COMPASS III force field was selected to define the reasonable distribution of potential energy among atoms, and the EPDM/ETFE polymer model was established. It consists of three components: bonding term, non bonding function and cross coupling term [46]. The total energy of its molecular system is shown in Eq. (1), as follows:

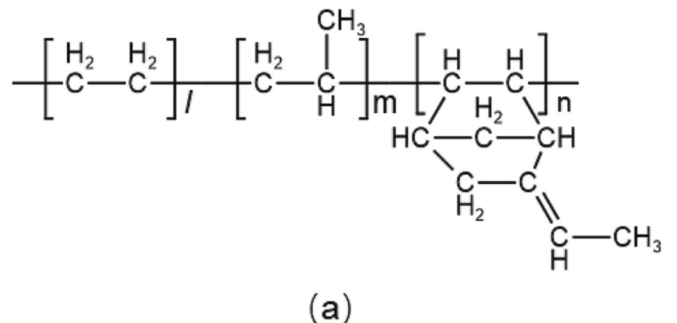
我们选择将 EPDM 与 ETFE 复合以改善聚合物材料的声学性能。

碳纳米结构，如单层碳纳米管、双层碳纳米管和碳纳米颗粒，在过去几十年中受到了极大关注，因为它们具有强大的机械性能，可以用作基体材料机械性能的增强剂[37–39]。虽然 EPDM 的机械性能低于 ETFE，但通过引入碳纳米结构，EPDM/ETFE 材料可以用于增强宏观性能。

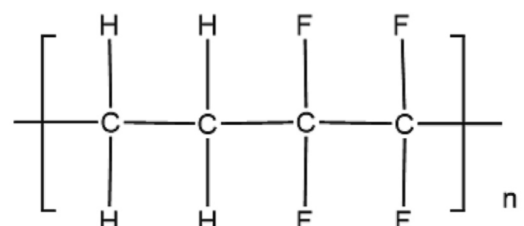
为了研究这种颗粒增强复合聚合物材料的力学性能，分子动力学 (MD) 被认为是一种非常有用的方法[40]，可以大大减少从材料设计阶段开始所需的工作量，并很好地计算聚合物与纳米填料材料之间的力学性能[41, 42]，并获得准确的宏观力学性能，为研究其声学性能提供必要的数据支持。

膜型声学超材料 (MAMs) 是一种可以针对特定频率范围进行有效隔音的结构类型[43]：通过设计，针对频率带可以出现在低频范围。因此，MAMs 的结构设计已经受到研究人员的深入和广泛研究。然而，关于 MAMs 声传输损失的理论研究仍然很少：文献[44]研究了质量块对 MAMs 声传输损失的影响；Langfeldt 等人[45]引入了一种基于网格收敛指数的方法来加快声传输损失的计算。

在这项研究中，EPDM、ETFE 和碳纳米结构首次混合，设计了 MAMs 结构的颗粒增强聚合物薄膜，以研究其机械和声学性能。因此，本研究首先使用 MD 方法计算颗粒增强 EPDM/ETFE 薄膜的机械性能。其次，基于离散点匹配方法构建了这种薄膜超材料声传输损失的预测模型。同时，利用 COMSOL Multiphysics 软件开发了声-结构耦合的有限元模型，以验证理论部分的准确性。最后，通过比较相等质量的聚合物薄膜和金属薄膜，验证了颗粒增强 EPDM/ETFE 薄膜声学超材料的隔音效果。同时，讨论了 7 种材料和结构参数，包括不同级别的微观-宏观参数，并分析了它们对声传输损失的影响规律。



(a)



(b)

图 1. EPDM (a) 和 ETFE (b) 的分子结构式。

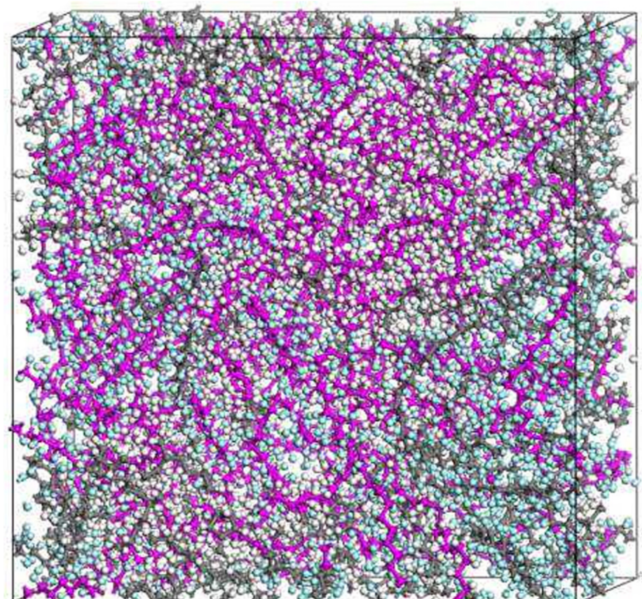


图 2. EPDM/ETFE 共混物的分子模型。

2. 分子动力学计算

2.1. 完整原子模型构建 EPDM 广泛应用于声音吸收/隔音材料的设计中，因其出色的声学性能。因此，在本研究中，选择 EPDM 和 ETFE 构建热塑性材料，以改善材料的声学性能，然后使用碳纳米颗粒进一步增强材料的机械性能，以提高复合材料的隔音效果。该材料由 BIOVIA Materials Studio 2020 提供的平台建模，其分子式如图 1 所示。

首先，建立了由 50% 四氟乙烯和 70% 乙烯、25% 丙烯、5% 乙烯基-去氢脱环戊二烯的乙烯丙烯共聚物分子链组成的 ETFE 分子链。然后，根据 EPDM: ETFE = 3:7 的组分比例，将这些聚合物装入周期性模拟盒中，如图 2 所示。

在 Materials Studio 2020 软件中使用 Force 模块进行几何结构优化，以获得合理的三维分子构型。在这个模块中，采用智能方法进行结构优化。在复合材料的构建过程中，使用软件中的非晶胞模块，并选择 COMPASS III 力场来定义原子间潜能能量的合理分布，并建立 EPDM/ETFE 聚合物模型。它由三个组成部分组成：键合项、非键合函数和交叉耦合项[46]。其分子系统的总能量如下所示：Eq. (1)。

$$E_{\text{tot}} = (E_b + E_\theta + E_\phi + E_\omega + E_c) + (E_h + E_e + E_v) \quad (1)$$

Where, E_b is the key length expansion vibration kinetic energy; E_θ is the bond angle bending vibration energy; E_ϕ is dihedral angle torsion energy; E_ω is the angular offset vibration energy outside the plane; E_c is the cross valence bond interaction energy; E_h is hydrogen bond interaction energy; E_e is electrostatic interaction energy; E_v is van der Waals interaction energy.

The carbon nanoparticles to be doped were then built in the shape of spherical carbon nanoparticles with a diameter of 5 Å. The carbon nanoparticles were doped into the EPDM/ETFE polymer model, all at a mass percentage of 1%. After the total energy minimisation of the system was obtained using the conjugate gradient method, the composites were optimised for molecular dynamics using the NVT (constant atomic number, constant volume, constant temperature) and NPT (constant atomic number, constant pressure, constant temperature) synthesis, respectively. In the NVT system, the temperature was set at 298 K with a step of 0.5 fs and 100 ps of relaxation to bring the model system to equilibrium. The final equilibrium system is used as the base model for subsequent performance calculations. The final equilibrium system was used as the base model for the subsequent property calculations (shown in Fig. 3). Finally, the macroscopic mechanical properties of the material were calculated by Forcite Model of Material Studio software, and the calculation flow is shown in Fig. 4, and the

Young's modulus and Poisson's ratio of the EPDM/ETFT composite polymer material were obtained.

2.2. Mechanical property calculation

The static constant strain method is used to apply a small strain within the elastic limit in a well balanced system, and then the energy optimization is performed again. Apply this strain to different directions and repeat the above process for many times to calculate the stiffness matrix of the model. Its element is the second derivative of potential energy to strain, as shown in Eq. (2):

$$C_{ij} = \frac{1}{V} \cdot \frac{\partial^2 U}{\partial \varepsilon_i \partial \varepsilon_j} = \frac{\partial \sigma_i}{\partial \varepsilon_j} = \frac{\sigma_+ - \sigma_-}{2\varepsilon_j} \quad (2)$$

Where, U is potential energy; σ is stress which is the first derivative of potential energy per unit volume to strain, "+" represents tension, and "-" represents compression; ε is strain.

For isotropic materials, the sum of the two Lame constants can be obtained from the stiffness matrix, as shown in Eq. (3).

$$\begin{cases} \lambda = \frac{1}{3}(C_{11} + C_{22} + C_{33}) - \frac{2}{3}(C_{44} + C_{55} + C_{66}) \\ \mu = \frac{1}{3}(C_{44} + C_{55} + C_{66}) \end{cases} \quad (3)$$

According to this, Young's modulus E , shear modulus G , bulk modulus B and Poisson's ratio ν are

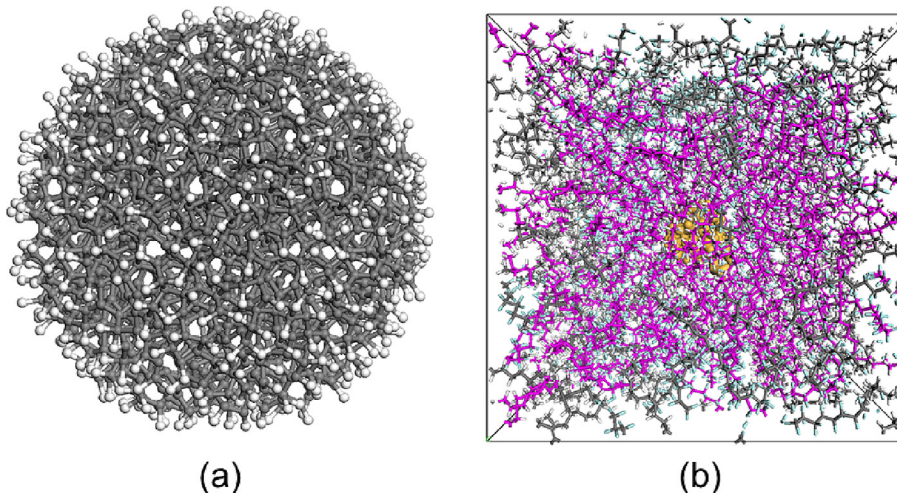


Fig. 3. The optimized structure of (a) Carbon nanoparticles, and (b) Particle enhanced EPDM/ETFE molecular model (the orange part in the middle is the carbon nanoparticles shown in Figure (a)). (For interpretation of the references to colour in this figure legend, the reader is referred to the web version of this article.)

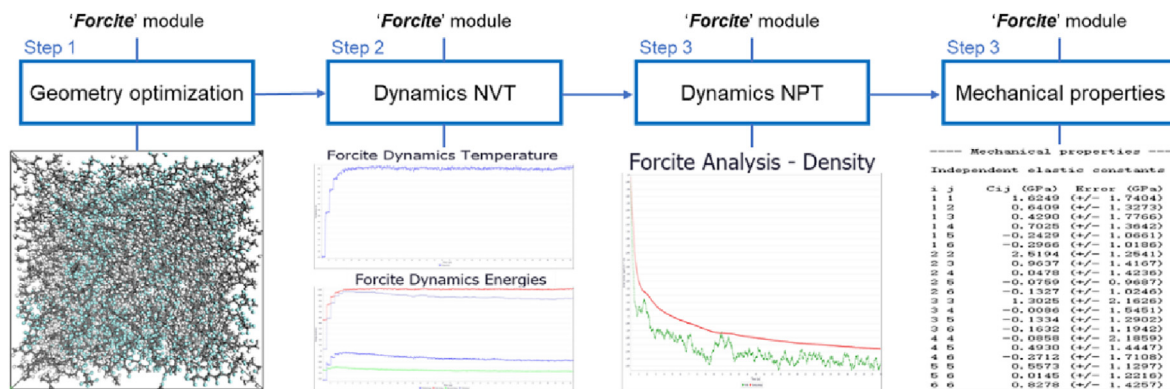


Fig. 4. The MD Simulation Process for Mechanical Properties of Particle Reinforced EPDM/ETFE Blends.

$$E = E_{\text{L}} + E_{\text{B}} + E_{\text{A}} + E_{\text{P}} + E_{\text{C}} + E_{\text{H}} + E_{\text{E}}$$

其中, E 是键长扩展振动动能; E 是键角弯曲振动动能; E 是二面角扭转能; E 是平面外角度偏移振动能; E 是交叉价键相互作用能; E 是氢键相互作用能; E 是静电相互作用能; E 是范德华相互作用能。

被掺杂的碳纳米颗粒随后被建造成直径为 5 埃的球形碳纳米颗粒。

这些碳纳米颗粒被掺杂到 EPDM/ETFE 聚合物模型中, 质量百分比均为 1%。在使用共轭梯度法获得系统的总能量最小化后, 分别使用 NVT (恒定原子数、恒定体积、恒定温度) 和 NPT (恒定原子数、恒定压力、恒定温度) 合成方法对复合材料进行分子动力学优化。在 NVT 系统中, 温度设定为 298K, 步长为 0.5fs, 进行 100ps 的弛豫以使模型系统达到平衡。最终的平衡系统被用作后续性能计算的基础模型。最终的平衡系统被用作后续性能计算的基础模型 (如图 3 所示)。最后, 通过 Material Studio 软件的 Forcite 模型计算了材料的宏观力学性能, 计算流程如图 4 所示。

EPDM/ETFE 复合聚合物材料的杨氏模量和泊松比已获得。

2.2. 机械性能计算 使用静态恒定应变法在一个良好平衡的系统中施加小应变, 然后再次进行能量优化。将这种应变应用于不同方向, 并重复上述过程多次, 以计算模型的刚度矩阵。其元素是势能对应变的二阶导数, 如方程 (2) 所示:

$$C = \frac{1}{V} \frac{\partial U}{\partial e} = \frac{\partial r}{\partial e} - \frac{r - r_0}{2e}$$

在这里, U 是势能; r 是应力, 是单位体积势能对应变的第一导数, “+”表示张力, “-”表示压缩; 对于各向同性材料, 两个拉梅常数的和可以从刚度矩阵中获得, 如方程 (3) 所示。

$$(k = \frac{1}{4} C_p C_b C_d) \quad p = \frac{C_p C_b C_d}{C_b} \quad \nu = \frac{C_b - C_d}{2(C_b + C_d)}$$

根据这个, 杨氏模量 E , 剪切模量 G , 体积模量 B 和泊松比 ν

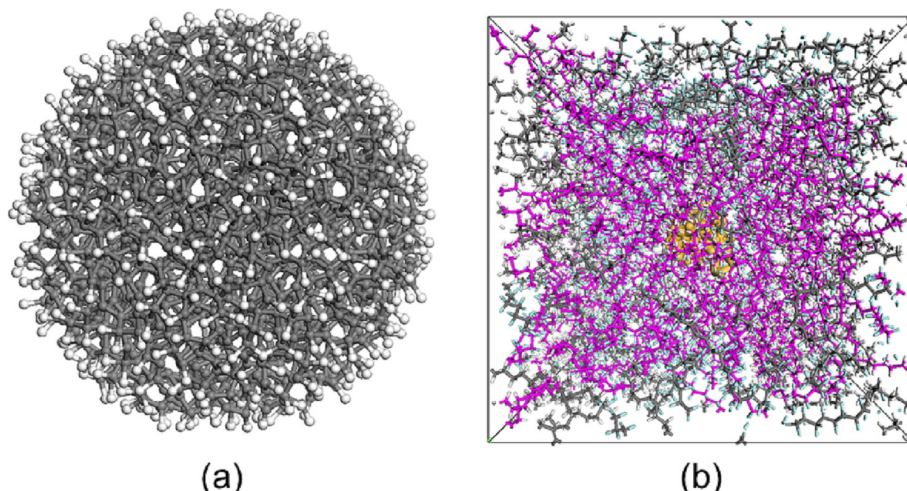


图 3. (a) 碳纳米颗粒的优化结构, 以及 (b) 颗粒增强的 EPDM/ETFE 分子模型 (中间的橙色部分是图(a)中显示的碳纳米颗粒)。(有关本图图例中颜色的解释, 请参阅本文的网络版本。)

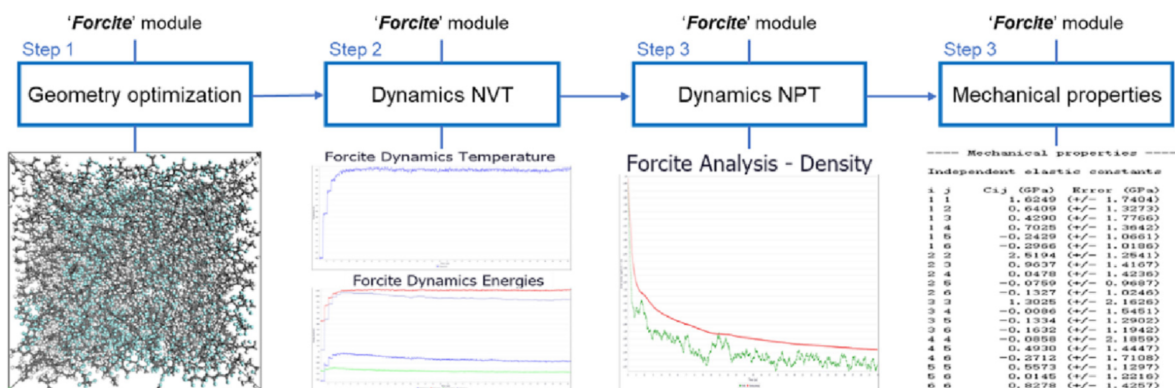


图 4. 粒子增强的 EPDM/ETFE 共混物力学性能的分子动力学模拟过程。

$$\begin{cases} E = \mu \cdot \frac{3\lambda+2\mu}{\lambda+\mu} \\ G = \mu \\ B = \lambda + \frac{2}{3}\mu \\ \nu = \frac{\lambda}{2(\lambda+\mu)} \end{cases} \quad (4)$$

3. Sound transmission loss of a polymer composite solid film metamaterial

In the literature [44,47,48], it is demonstrated through experiments, simulations and other methods that a single acoustic metamaterial cell can extrapolate the sound transmission loss characteristics (variation trend, optimal frequency range, etc.) of periodic structures, but there will be small fluctuations in amplitude. Therefore, we choose a cell of MAMs to establish a theoretical model.

3.1. Structure of polymer solid films containing carbon nanoparticles

As shown in Fig. 5, this kind of film metamaterial takes EDPM/ETFT polymer material as the base material of the film, carbon nanoparticles as the reinforcement of the film, and a mass block of structural steel is attached above the film. The thickness of the square film is 0.025 mm, and the side length is 25 mm; the mass block is a cylindrical structure with a radius of 2 mm and a height of 2 mm.

3.2. Sound transmission loss

The rectangular film of the loaded mass block is shown in Fig. 6. The origin of the coordinates is located at one corner of the rectangular film. The x-axis and y-axis coincide with the lengths of both sides of the rectangle, respectively. The side lengths are L_x and L_y . The periphery of the film is fixed, its surface density is m_M , and the uniform tension force of T acts on the inside of the film. The geometric shape of the additional mass block is a cylinder, its center is located in the center of the film, and the height of the mass block is h_m . The vibration of the membrane can be described by Helmholtz equation as follows:

$$m_M \frac{\partial^2}{\partial t^2} w(x, y, t) - T \nabla^2 w(x, y, t) = P(x, y, t) + f_m(x, y, t) \quad (5)$$

Where, $\nabla^2 = \partial^2 / \partial x^2 + \partial^2 / \partial y^2$ is the Laplace operator, $w(x, y, t)$ is the lateral displacement of the film surface, $P(x, y, t)$ is the sound pressure acting on the film, and $f_m(x, y, t)$ is the coupling force generated by the load mass block, and their expressions are

$$w(x, y, t) = \hat{w}(x, y) e^{i\omega t}$$

$$P(x, y, t) = \hat{P}(x, y) e^{i\omega t}$$

$$f_m(x, y, t) = \hat{f}_m(x, y) e^{i\omega t}$$

Where, \hat{w} is the amplitude of transverse vibration, \hat{P} is the amplitude of sound pressure, and \hat{f}_m is the amplitude of additional mass coupling force. For convenience of expression, we introduce dimensionless parameters:

$$\xi = x/L_x \quad \eta = y/L_y \quad \zeta = z/L_z \quad u = \hat{w}/L_x$$

$$\Lambda = L_x/L_y \quad \beta = \hat{P}L_x/Tk^2 = m_M\omega^2 L_x^2/T \quad \gamma = \hat{f}_m/(TL_x)$$

Eq. (5) can be converted into dimensionless form, as shown in Eq. (6).

$$-k^2 u - u_{\xi\xi} - \Lambda^2 u_{\eta\eta} = \beta + \gamma \quad (6)$$

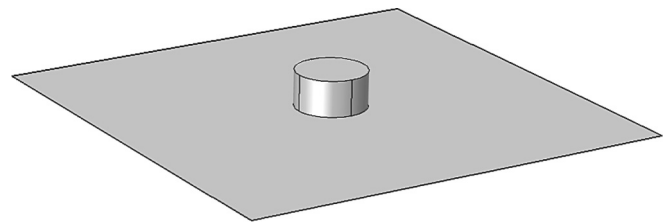


Fig. 5. MAM structure of particle reinforced polymer.

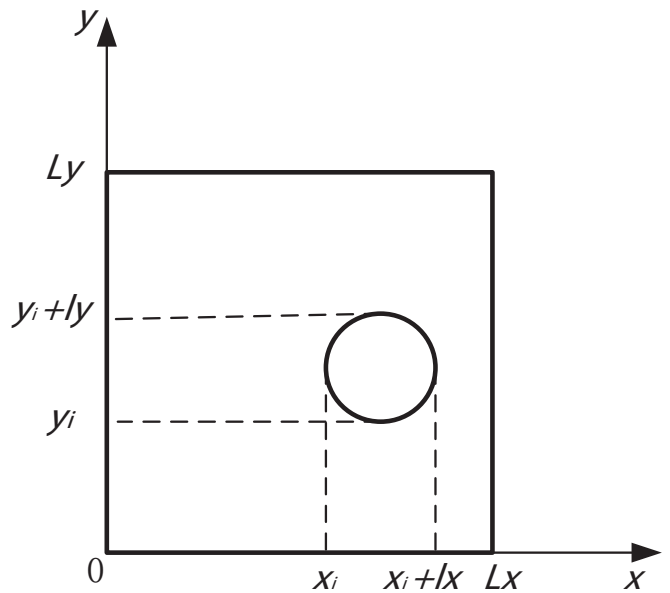


Fig. 6. Additional distributed mass on the film surface at fixed constraints.

Where, $u_{\xi\xi}$ and $u_{\eta\eta}$ are the second derivative of u with respect to ξ and η .

For the amplitude of the added mass force γ , it can be approximately expressed as the sum of the force amplitude of a group of discrete points(γ_i) using the point matching method:

$$\gamma = \sum_{i=1}^I \gamma_i \delta(\xi - \xi_i) \delta(\eta - \eta_i) \quad (7)$$

Where I is the total number of matching points, γ_i is the dimensionless force amplitude of the i th matching point, ξ_i and η_i is the coordinate of the i th matching point, δ is Dirac function.

In order to solve Eq. (7), u needs to be approximately expressed as

$$u = \sum_{nx=1}^{Nx} \sum_{ny=1}^{Ny} q_n \sin(nx\pi\xi) \sin(ny\pi\eta) \quad (8)$$

Where Nx and Ny are the number of modes in the x and y directions respectively, and $N = NxNy$. Therefore, Eq. (6) can be surface integrated and rewritten as a matrix, as shown in Eq. (9).

$$(\mathbf{C} - k^2 \mathbf{M}) \mathbf{q} = \beta \mathbf{b} + \mathbf{L} \gamma \quad (9)$$

Where \mathbf{C} is the stiffness matrix, \mathbf{M} is the mass matrix, \mathbf{L} is the matching point matrix, and \mathbf{b} is the force vector.

To obtain the specific expression of the force vector at the coupling point, it is necessary to describe the motion of the added mass. A local coordinate system is introduced for each mass, and its origin is the center of mass of the added mass. When the added

8 E ¼ 1 □
 $\zeta \frac{1}{4} 1$
 $\geq B \frac{1}{4} k p 1$
 $V \frac{1}{4}$

δ4P

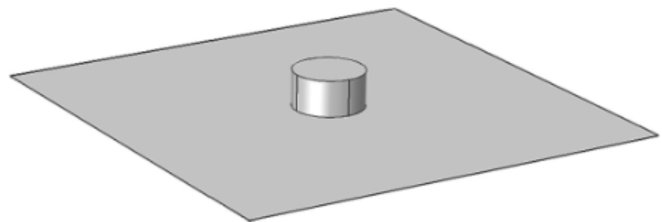


图 5. 颗粒增强聚合物的 MAM 结构。

3. 聚合物复合固体薄膜超材料的声传输损失

在文献[44, 47, 48]中, 通过实验、模拟和其他方法证明, 单个声学超材料单元可以推断周期结构的声传输损耗特性(变化趋势、最佳频率范围等), 但振幅会有小幅波动。因此, 我们选择 MAMs 的单元建立理论模型。

3.1. 含碳纳米颗粒的聚合物固体薄膜结构 如图 5 所示, 这种薄膜超材料以 EDPM/ETFT 聚合物材料作为薄膜的基材, 碳纳米颗粒作为薄膜的增强材料, 并在薄膜上方附加了一个结构钢的质量块。正方形薄膜的厚度为 0.025 毫米, 边长为 25 毫米; 质量块是一个半径为 2 毫米, 高度为 2 毫米的圆柱结构。

3.2. 声传输损失 负载质量块的矩形薄膜如图 6 所示。坐标原点位于矩形薄膜的一个角落。x 轴和 y 轴分别与矩形的两边长度重合。边长分别为 L_x 和 L_y 。薄膜的周长固定, 其表面密度为 m , 薄膜内部受到均匀张力 T 的作用。附加质量块的几何形状为圆柱体, 其重心位于薄膜中心, 质量块的高度为 h 。薄膜的振动可以用亥姆霍兹方程描述如下:

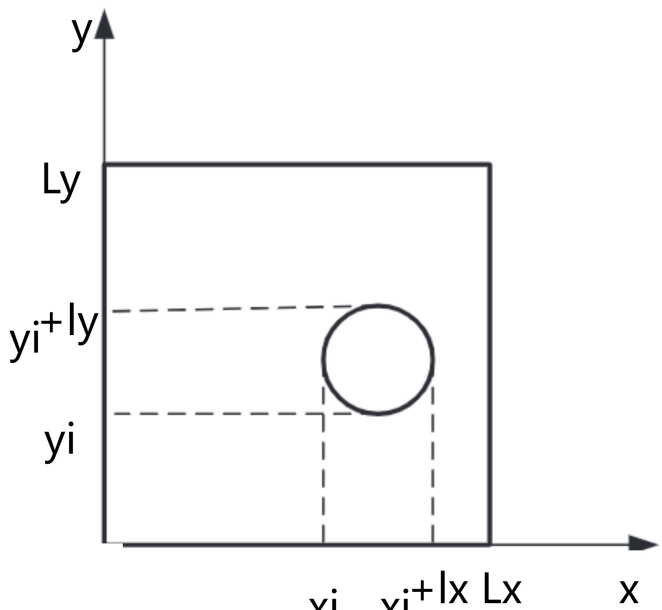


图 6. 在固定约束条件下, 薄膜表面上的额外分布质量。

$$m \frac{\partial^2 w(x, y, t)}{\partial t^2} = Trw(x, y, t) - P(x, y, t) - f(x, y, t) \quad \text{δ5P}$$

在这里, $\frac{\partial^2}{\partial t^2} w(x, y, t)$ 是拉普拉斯算子, $w(x, y, t)$ 是薄膜表面的横向位移, $P(x, y, t)$ 是作用在薄膜上的声压力, $f(x, y, t)$ 是由负载块产生的耦合力, 它们的表达式为

$$w(x, y, t) = \hat{w}(x, y) e^{j\omega t} \quad \text{δ6P}$$

$$P(x, y, t) = \hat{P}(x, y) e^{j\omega t} \quad \text{δ7P}$$

$$f(x, y, t) = \hat{f}(x, y) e^{j\omega t} \quad \text{δ8P}$$

在这里, \hat{w} 是横向振动的幅度, \hat{P} 是

声-质量耦合力的振幅。为了方便表达, 我们引入无量纲参数:

$$\begin{aligned} n &\equiv \frac{x}{L_x}, y \equiv \frac{y}{L_y}, z \equiv \frac{z}{L_z}, u \equiv \frac{w}{L}, \\ K &\equiv \frac{Tr}{L_x^2}, P \equiv \frac{P}{L_x^2}, f \equiv \frac{f}{L_x^2}, \end{aligned} \quad \text{δ9P}$$

方程 (5) 可以转换为无量纲形式, 如方程 (6) 所示。

$$ku_{nn} = K \hat{u}_{nn} + P_{nn} + f_{nn} \quad \text{δ6P}$$

在这里, u_{nn} 和 u_{nn} 是 u 相对于 n 的二阶导数, 对于添加质量力 c 的振幅, 可以近似表示为使用点匹配方法的一组离散点的力振幅之和 (c):

$$c \equiv \sum_i c_i d_{ni} \quad \text{δ7P}$$

其中 I 是匹配点的总数, c_i 是第 i 个匹配点的无量纲力振幅, n_i 和 g_i 是第 i 个匹配点的坐标, d_i 是 Dirac 函数。

为了解决方程 (7), 需要将 u 近似表示为

$$u \approx \sum_{n_x=1}^{N_x} \sum_{n_y=1}^{N_y} q \sin(n_x \pi x / L_x) \sin(n_y \pi y / L_y) g_i \quad \text{δ8P}$$

其中, N_x 和 N_y 分别是 x 和 y 方向的模式数, $N = N_x N_y$ 。因此, 方程 (6) 可以进行表面积分并重写为矩阵, 如方程 (9) 所示。

$$\delta C = kM\hat{q} \quad \text{δ9P}$$

C 是刚度矩阵, M 是质量矩阵, \hat{q} 是匹配点矩阵, b 是力向量。

为了获得耦合点处力矢量的具体表达, 需要描述附加质量的运动。为每个质量引入一个本地坐标系, 其原点是附加质量的质心。当附加。

mass interacts with the film and moves, the displacement of any matching point on the added mass can be expressed by Eq. (10).

$$u_M = u_S - \alpha_\xi \xi' + \alpha_\eta \eta' \quad (10)$$

Where u_S is the centroid displacement, α_ξ and α_η are the rotation angle of the mass around the coordinate axes x' and y' , respectively, ξ' and η' are the coordinates in the local coordinate system.

Then, by coupling the displacement amplitude of the film part and the additional mass part at each matching point, Eq. (11) is obtained.

$$u_M(\xi', \eta') = u(\xi, \eta) \quad (11)$$

Convert it to matrix form, as shown in Eq. (12).

$$-\mathbf{L}^T \mathbf{q} + \frac{1}{k^2} \mathbf{G} \gamma = \mathbf{0} \quad (12)$$

Eq. (9) and (12) can form a system of Eq. (13):

$$\begin{bmatrix} C - k^2 M & -L \\ -L^T & \frac{1}{k^2} G \end{bmatrix} \begin{pmatrix} q \\ \gamma \end{pmatrix} = \beta \begin{pmatrix} b \\ 0 \end{pmatrix} \quad (13)$$

The Homogeneous form of this equation group is a generalized eigenvalue problem. Its solution is referred to [45,49], and the modal contribution factor \mathbf{c} is obtained:

$$\mathbf{c} = \beta (\Lambda - k^2 \mathbf{I})^{-1} (\mathbf{X}^T \mathbf{B} \mathbf{X})^{-1} \mathbf{X}^T \begin{bmatrix} \mathbf{b} \\ \mathbf{0} \end{bmatrix} \quad (14)$$

Where Λ is the diagonal matrix composed of the characteristic value k_i^2 of the mass film system.

Under the sub wavelength condition, the acoustic radiation behavior of the structure is mainly determined by the average vibration amplitude of its surface or the piston motion. Under this condition, the membrane can be regarded as a rigid wall with an effective surface mass density, which can be calculated as a function of the excitation frequency:

$$m' = -\frac{m_M}{k^2 [\mathbf{b}^T \ 0] \mathbf{X} \mathbf{c}} \quad (15)$$

According to the mass law, the sound transmission coefficient (Eq. (16)) and the sound transmission loss (Eq. (17)) can be calculated.

$$t = \frac{1}{1 + \frac{i \omega m'}{2 \rho_0 c_0}} \quad (16)$$

$$TL = -20 \log_{10} |t| \quad (17)$$

Where, ρ_0 and c_0 are the density and sound velocity of the medium that transmits sound waves.

4. Model validation

For the polymer film metamaterial shown in Fig. 5, the multi physical field simulation software COMSOL5.6 is used for simulation verification: the mechanical properties of the material are obtained by molecular dynamics, the membrane material is composed of structural steel, EPDM and ETFE, and the mass block is structural steel. Parameters of structural steel and carbon nanoparticles are shown in Table 1, and membrane parameters are shown in Table 2.

4.1. Accuracy verification of sound transmission loss

Select the acoustic structure coupling module in COMSOL5.6, and measure the sound insulation of the structure by simulating

Table 1
Material parameter table.

Material	Young's modulus (E)	Poisson's ratio (nu)	Density (ρ)
EPDM	7.8 MPa	0.47	880 kg/m ³
ETFE	0.755 GPa	0.42	1750 kg/m ³
Carbon nanoparticles	336 GPa	0.304	1500 kg/m ³
Structural steel	210 GPa	0.30	7860 kg/m ³

Table 2
Simulation results of membrane material parameters.

Elastic properties	MD result
Young's modulus, E(GPa)	1.1636
Poisson's ratio (nu)	0.34
Density, ρ(kg/m ³)	1346
Stiffness coefficient, Cij (GPa)	
C ₁₁	1.6249
C ₂₂	2.5194
C ₃₃	1.3025
C ₄₄	-0.0858
C ₅₅	0.5573
C ₆₆	0.8278

the impedance tube to measure the transmission loss as described in [44]. The EPDM/ETFE polymer film reinforced by carbon nanoparticles is surrounded by fixed constraints, and a 25 mm high cavity is set above and below it respectively to eliminate near-field effects, as shown in Fig. 7 (a). The plane wave radiation condition is used to incident a uniform sound pressure of 1 Pa along the normal direction, and the average sound pressure is received on the exit surface to obtain its STL. The corresponding STL calculation is given by the Eq. (18).

$$TL = 20 \lg(P_{in}/P_{out}) \quad (18)$$

where $P_{in} = 1$ Pa and P_{out} is shown in Eq. (19).

$$P_{out} = \frac{\int_s |P_t| ds}{s} \quad (19)$$

At the same time, the MD simulation method based on Material Studio 2020 is combined with the discrete point matching method to theoretically analyze the sound insulation characteristics of this polymer film metamaterial, and the results are verified with the finite element results of the acoustic solid coupling model, as shown in Fig. 7 (b). In the results of this figure, it is obvious that the transmission loss calculated by the two methods has the same change and is highly coincident, which proves the accuracy of the theoretical method. There are differences in 300 Hz because the theory ignores the influence of edge effect caused by fixed perimeter on sound insulation. However, it can be seen that except for the 200 Hz-400 Hz frequency band, this structure has good sound insulation performance in other frequency bands, which greatly enhances the poor acoustic performance of ETFE film in traditional structures, and has the potential of strong sound insulation performance in low-frequency broadband.

It should be emphasized that both methods reflect that there is a peak of the sound transmission loss curve at about 430 Hz. Combining with the membrane surface vibration velocity diagram at the valley (265 Hz) and peak (430 Hz) of the sound transmission loss curve in Fig. 7 (b), it can be found that: at the peak, the surface vibration is mainly concentrated on the mass block, and the membrane surface vibration is very small. However, near the valley value, there is a large area with a certain amplitude on the film, and there is a tendency to transfer surface vibration around the mass block. Therefore, the structure at 430 Hz can well block the

质量与薄膜相互作用并移动，附加质量上任何匹配点的位移可以用方程 (10) 表示。

$$u^{1/4} u = a n \beta a g$$

δ10p

质心位移在坐标轴' 和 y' 周围的质量的运动角度，分别是 n' 和 g 在本地坐标系中的坐标。

然后，通过在每个匹配点上耦合薄膜部分的位移幅度和额外质量部分，得到方程 (11)。

$$u \ddot{u}; g \ddot{p} \frac{1}{4} u \ddot{u}; g \ddot{p}$$

δ11p

将其转换为矩阵形式，如公式 (12) 所示。

I'm sorry, but the source text you provided seems to be incomplete or corrupted. Could you please provide a valid source text for translation into Simplified Chinese?

方程 (9) 和 (12) 可以构成方程组 (13)：

$$\begin{matrix} C & kM & L \\ L & \frac{1}{k} G & C \end{matrix} \begin{matrix} \# \\ q \\ 0 \end{matrix} \begin{matrix} \square \\ \square \\ \square \\ \square \\ b \\ 0 \end{matrix} \quad \delta 13p$$

这个方程组的齐次形式是一个广义特征值问题。它的解参考文献 [45, 49]，模态贡献因子 c 如下获得：

$$c^{\frac{1}{4}} b K \square k l \quad X B X \quad X \quad b \quad 0 \quad \delta 14p$$

K 是由质量薄膜系统的特征值 k 组成的对角矩阵。

在次波长条件下，结构的声辐射行为主要由其表面的平均振幅或活塞运动决定。在这种条件下，膜可以被视为具有有效表面质量密度的刚性墙壁，该密度可以作为激励频率的函数进行计算：

$$m^{\frac{1}{4}} \frac{1}{kb} \quad m \quad 0 \quad X_c \quad \delta 15p$$

根据质量法则，可以计算声传输系数（方程 (16)）和声传输损失（方程 (17)）。

$$t^{\frac{1}{4}} \frac{1}{1 \beta} \quad \delta 16p$$

$$TL \frac{1}{4} \square 20 \log jtj \quad \delta 17p$$

传声波的介质的密度和声速。

4. 模型验证 对于图 5 中显示的聚合物薄膜超材料，使用多物理场模拟软件 COMSOL5.6 进行模拟验证：材料的力学性能通过分子动力学获得，膜材料由结构钢、EPDM 和 ETFE 组成，质量块为结构钢。结构钢和碳纳米颗粒的参数如表 1 所示，膜参数如表 2 所示。

4.1. 声传输损失的准确性验证 在 COMSOL5.6 中选择声学结构耦合模块

表 1
材料参数表。

材料	Young's 模量 (E)	泊松的比率 (nu)	密度 (q)
EPDM	7.8 兆帕	0.47	880 公斤/米
ETFE	0.755 GPa	0.42	1750 公斤/米
碳纳米颗粒	336 GPa	0.304 1500 kg/m	结构钢 210 GPa 0.30 7860 kg/m

表 2
膜材料参数的模拟结果。

弹性特性	MD 结果
杨氏模量, E (GPa)	1.1636
泊松比 (v)	0.34
刚度系数, Cij (GPa)	C 1.6249
	C 2.5194
	C 1.3025
	C 0.0858
	C 0.5573
	C 0.8278

通过模拟阻抗管测量传输损耗来测量结构的隔音性能，如[44]所述。由碳纳米颗粒增强的 EPDM/ETFE 聚合物薄膜被固定约束包围，上下分别设置一个 25 毫米高的腔室以消除近场效应，如图 7(a) 所示。采用平面波辐射条件沿法线方向入射均匀声压 1 帕，接收出口表面的平均声压以获得其 STL。相应的 STL 计算由方程(18)给出。

$$TL = 20 \lg P = P \quad \delta 18p$$

在这里 $P = 1$ Pa， P 在方程 (19) 中显示。

$$P^{\frac{1}{4}} \int_{-\infty}^{\infty} ds \quad \delta 19p$$

同时，基于 Materail Studio 2020 的 MD 模拟方法与离散点匹配方法相结合，理论分析了这种聚合物薄膜超材料的隔音特性，并将结果与声固耦合模型的有限元结果进行验证，如图 7 (b) 所示。从这幅图的结果可以明显看出，两种方法计算的传输损耗变化相同且高度一致，证明了理论方法的准确性。在 300 Hz 处存在差异，因为理论忽略了固定周边对隔音的边缘效应的影响。然而，除了 200 Hz~400 Hz 频段外，可以看出在其他频段，这种结构具有良好的隔音性能，大大增强了传统结构中 ETFE 薄膜的差劲声学性能，并具有在低频宽带中强大隔音性能的潜力。

应强调的是，两种方法都反映出声传输损失曲线在大约 430 赫兹处有一个峰值。结合图 7 (b) 中声传输损失曲线在谷值 (265 赫兹) 和峰值 (430 赫兹) 处的膜表面振动速度图，可以发现：在峰值处，表面振动主要集中在质块上，而膜表面振动非常小。然而，在接近谷值处，膜上有一个具有一定振幅的大面积，并且有一种将表面振动传递到质块周围的趋势。因此，在 430 赫兹处的结构可以很好地阻挡声音传输。

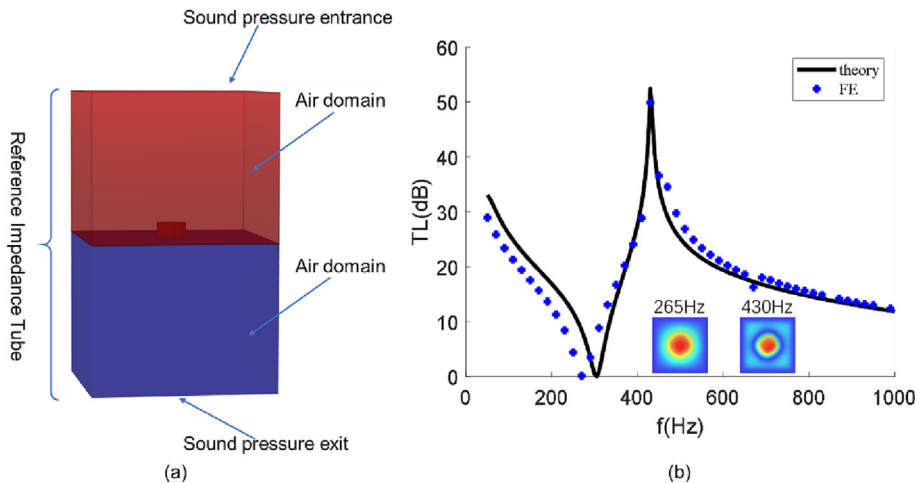


Fig. 7. Particle enhanced EPDM/ETFE MAM acoustic structure multi physical field simulation model: (a) acoustic structure coupling geometry; (b) Comparison of theoretical prediction and FE calculation results of sound transmission loss.

sound propagation, while there is a lot of sound transmission near the valley value.

4.2. Effectiveness analysis

In order to illustrate the effectiveness of this polymer film metamaterial, its sound transmission loss is compared with similar common structures of four different materials, including particle reinforced EPDM/ETFE film with the same substrate area and the same mass (tension 120 N/m), structural steel plate, homogeneous particle reinforced EPDM/ETFE polymer film and MAM of PEI material [50]. Fig. 8 shows the sound transmission loss of these five structures when the plane wave is perpendicular to the incident direction.

It can be seen from the figure that the sound insulation characteristic curve of this particle reinforced film metamaterial is completely different from the other three pure film structures: there is an obvious high sound insulation frequency band in this curve, and then the sound transmission loss starts to decrease with the increase of frequency, while the other three curves increase with the increase of frequency. Based on the sound transmission loss

curve of particle reinforced polymer film with equal area and mass, the sound insulation effect of polymer metamaterial structure is better than that of pure polymer film in the whole low frequency band. With the iron film as the benchmark, the sound insulation effect of membrane structures with equal mass is almost consistent, meeting the mass law. However, compared with the metamaterial structure, its sound insulation effect has the advantage that its sound insulation is also increasing with the increase of frequency. But in the low frequency band, especially in the range of 300 Hz–700 Hz, it is inferior to the metamaterial structure. Compared with the MAM of PEI material, the particle reinforced EPDM/ETFE material has greater average sound insulation and slower attenuation of sound transmission loss, but the PEI material will reach the frequency of the sound insulation peak earlier.

The advantage of this particle reinforced polymer film metamaterial is that it enhances the low-frequency stage that is more sensitive to human perception. In general, in the frequency band of 1000 Hz, the sound insulation effect of this structure is better than that of metal structures and polymer films of the same quality. This is mainly caused by local resonance, which makes the surface density of the structure change with frequency, as shown in Fig. 9: there is an extreme value near 430 Hz, which changes the change characteristics of the sound transmission loss curve, so there will be a sound insulation peak at this frequency.

5. Results and discussion

In this section, based on the proposed semi analytical method combining molecular dynamics simulation and discrete point matching method, the sound transmission loss of carbon containing nanoparticles reinforced polymer solid film metamaterial is predicted. The calculation method of its physical parameters is described in detail in Section 2. The influence of mass fraction of carbon nanoparticles, component ratio of polymer solid film, matrix attribute and mass block on sound transmission loss was discussed by using control variable method.

5.1. Influence law of carbon nanoparticle mass fraction

Carbon nanoparticles are selected from the carbon nanoparticles that are consistent with the multi physical field coupling simulation, and its diameter is $d = 5 \text{ \AA}$. Here, the sound transmission loss of MAM prepared by particle reinforced EPDM/ETFE polymer film with mass fraction of 1 wt%, 3 wt%, 5 wt% and 7 wt% is

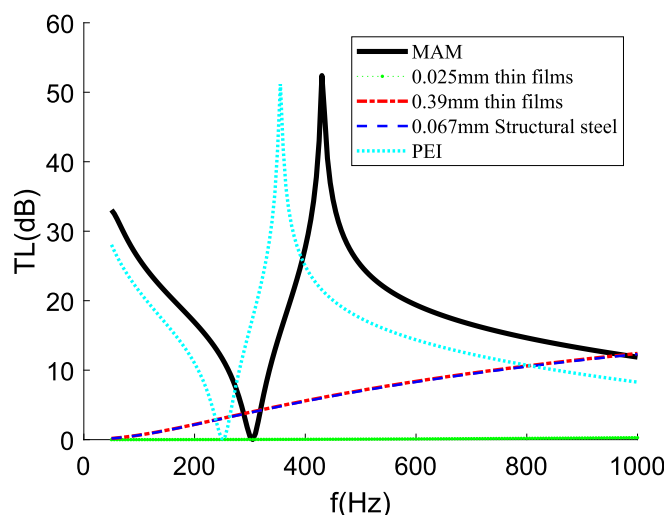


Fig. 8. Comparison of sound insulation performance between particle reinforced polymer MAM and four comparative structures.

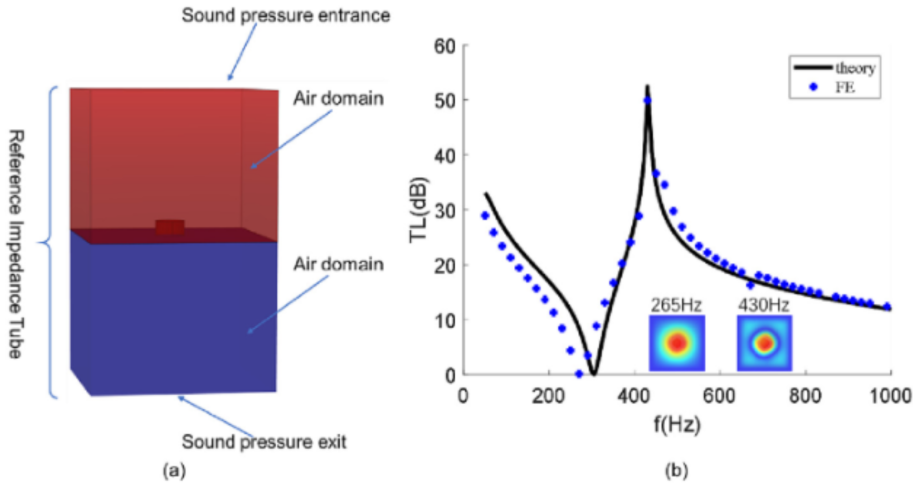


图 7. 颗粒增强的 EPDM/ETFE MAM 声学结构多物理场模拟模型: (a) 声学结构耦合几何; (b) 声传输损失的理论预测与有限元计算结果比较。

声音传播, 山谷附近有很多声音传输。

4.2. 效果分析 为了说明这种聚合物薄膜超材料的有效性, 将其声传输损失与四种不同材料的类似常见结构进行比较, 包括具有相同基底面积和相同质量 (张力 120 N/m) 的颗粒增强的 EPDM/ETFT 薄膜、结构钢板、均匀颗粒增强的 EPDM/ETFT 聚合物薄膜和 PEI 材料的 MAM [50]。图 8 显示了这五种结构在平面波垂直于入射方向时的声传输损失。

从图中可以看出, 这种颗粒增强薄膜超材料的隔音特性曲线与其他三种纯膜结构完全不同: 在这条曲线中有一个明显的高隔音频带, 随着频率的增加, 声传输损失开始减小, 而其他三条曲线则随着频率的增加而增加。

基于具有相等面积和质量的颗粒增强聚合物薄膜的声传输损失曲线, 聚合物超材料结构在整个低频段的隔音效果优于纯聚合物薄膜。以铁膜为基准, 具有相等质量的膜结构的隔音效果几乎一致, 符合质量定律。然而, 与超材料结构相比, 其隔音效果具有优势, 随着频率的增加, 其隔音也在增加。但在低频段, 特别是在 300 Hz 至 700 Hz 范围内, 它不如超材料结构。与 PEI 材料的 MAM 相比, 颗粒增强 EPDM/ETFT 材料具有更高的平均隔音和声传输损失的衰减速度较慢, 但 PEI 材料将更早达到隔音峰值频率。

这种颗粒增强聚合物薄膜超材料的优势在于增强了对人类感知更敏感的低频阶段。一般来说, 在 1000 赫兹频段, 这种结构的隔音效果比金属结构和同质量的聚合物薄膜更好。这主要是由于局部共振引起的, 使结构的表面密度随频率变化, 如图 9 所示: 在 430 赫兹附近有一个极值, 改变了声传输损失曲线的变化特性, 因此在这个频率会出现隔音峰值。

5. 结果与讨论 在本节中, 基于提出的将分子力学模型和离散点匹配方法相结合的半解析方法, 预测了含碳纳米颗粒增强聚合物固体薄膜超材料的声传输损失。其物理参数的计算方法在第 2 节中详细描述。通过使用控制变量方法, 讨论了碳纳米颗粒质量分数、聚合物固体薄膜成分比、基体属性和质量块对声传输损失的影响。

5.1. 碳纳米颗粒质量分数的影响规律 碳纳米颗粒是从与多物理场耦合模拟一致的碳纳米颗粒中选择的, 其直径为 $d = 5 \text{ \AA}$ 。在此, 由质量分数为 1 wt%、3 wt%、5 wt% 和 7 wt% 的颗粒增强的 EPDM/ETFE 聚合物薄膜制备的 MAM 的声传输损失为

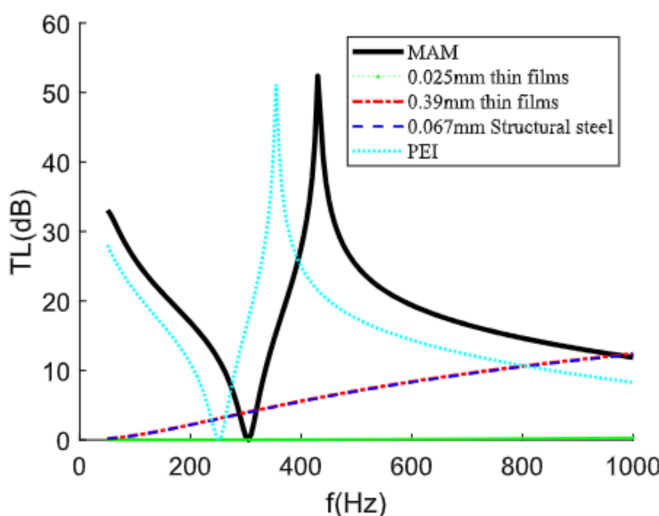


图 8. 颗粒增强聚合物 MAM 和四种比较结构之间隔音性能的比较。

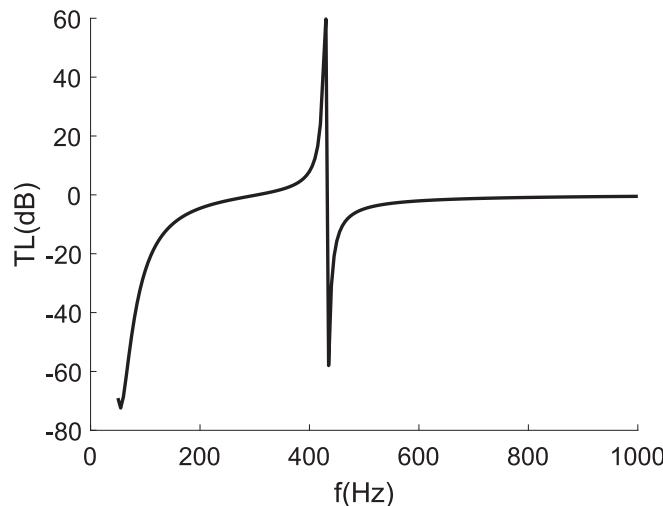


Fig. 9. Variation of surface density of particle reinforced polymer films with frequency.

compared. The mechanical parameters obtained by MD calculation are shown in Table 3, and the sound insulation results are shown in Fig. 10.

In Fig. 10, as the mass fraction of carbon nanoparticles increases, the average sound transmission loss increases and the frequencies where the peak and trough values of sound insulation are located are shifted towards higher frequencies. Without taking into account the effect of the shift in the sound transmission loss curve, it is also noticeable that the amplitude of the sound transmission loss curve is enhanced after 600 Hz with a larger mass fraction of carbon nanoparticles. In contrast, the sound transmission loss curves for the 3 wt%, 5 wt% and 7 wt% particle-enhanced MAM show only a slight shift in the two curves due to the small change in their mechanical properties (as can be seen from Table 3). At the same time, it can be found from the table that the film density has the greatest impact on the performance of the sound insulation curve (1 wt% and 3 wt% have the largest changes), and the Young's modulus and Poisson's ratio have little impact on the frequency of the sound insulation peak after reaching a certain value (as shown in the 5 wt% and 7 wt% curves).

5.2. Effects of polymer solid film

5.2.1. Impact trend with material composition

The proportion of different materials in composite materials often determines the macro mechanical properties of materials. Based on molecular dynamics, three theoretical models with increasing ETFE/EPDM ratio have been established. The mechanical parameters of each theoretical model of composite materials are shown in Table 4, and the characteristics of sound transmission loss are shown in Fig. 11.

It can be seen from the five curves that with the increase of the proportion of EPDM in the composite film, the peak and valley of sound insulation shift to low frequency, but the attenuation speed

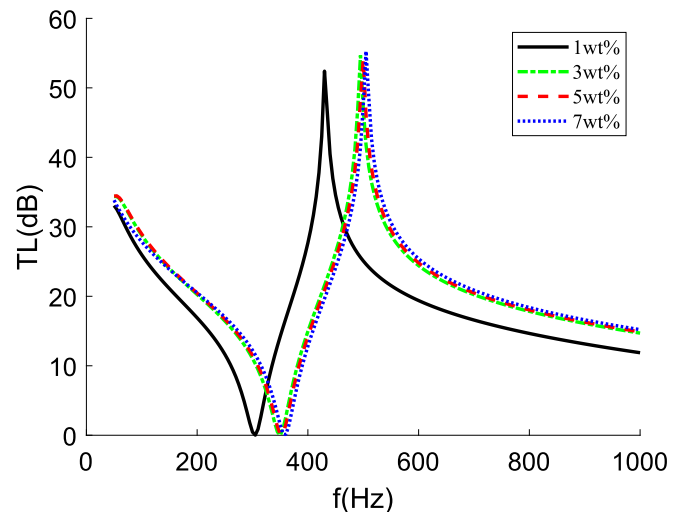


Fig. 10. Variation of sound transmission loss of particle reinforced EPDM/ETFE MAM with carbon nanoparticle mass fraction.

of sound transmission loss is relatively fast; The transmission loss amplitude decreases slightly with the increase of ETFE ratio. Therefore, it is an effective way to improve the acoustic performance of the structure by reasonably increasing the composition of EPDM in ETFE materials.

5.2.2. Change rule with thickness

For the particle reinforced EPDM/ETFE film metamaterial, the film thickness is called the substrate height h . A theoretical model of $h=(0.020, 0.025, 0.030)$ mm is established, and the corresponding sound transmission loss characteristics are analyzed. The results are shown in the Fig. 12.

As can be seen from the diagram, increasing the base height not only increases the average sound insulation size of the structure, but also shifts the insulation peak towards higher frequencies. This can therefore be a conventional method of adjusting the frequency band of the sound insulation due to changes in the global local resonance frequency as well as changes in the path of sound wave propagation.

5.2.3. Regular pattern of side length

The change of cell side length will change the overall metamaterial size, leading to the change of sound transmission loss. Increase the side length from 20 mm to 30 mm at 5 mm intervals. First, establish the corresponding theoretical model, and then calculate the sound transmission loss. The prediction results are shown in the Fig. 13.

As shown in Fig. 13, with the increase of side length, the sound insulation peak moves to low frequency, but the sound insulation effect in wide frequency band decreases with the increase of cell size. This is because the concentrated mass represented by the position of the center of mass is the largest in the cell. The farther away from the center of mass, the greater its vibration will be, making sound easier to spread and the worse the transmission loss

Table 3

Mechanical parameters of materials with different mass fractions of carbon nanoparticles.

Elastic properties	Carbon nanoparticles			
	1 wt%	3 wt%	5 wt%	7 wt%
Young's modulus, E(GPa)	1.1636	1.4948	1.8244	2.4093
Poisson's ratio (nu)	0.34	0.40	0.43	0.44
Density, ρ (kg/m ³)	1346	1354	1356	1362

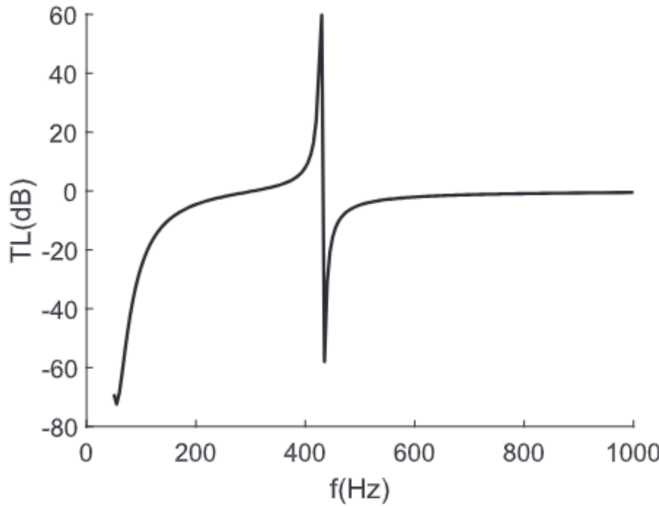


图 9. 频率变化下颗粒增强聚合物薄膜的表面密度变化。

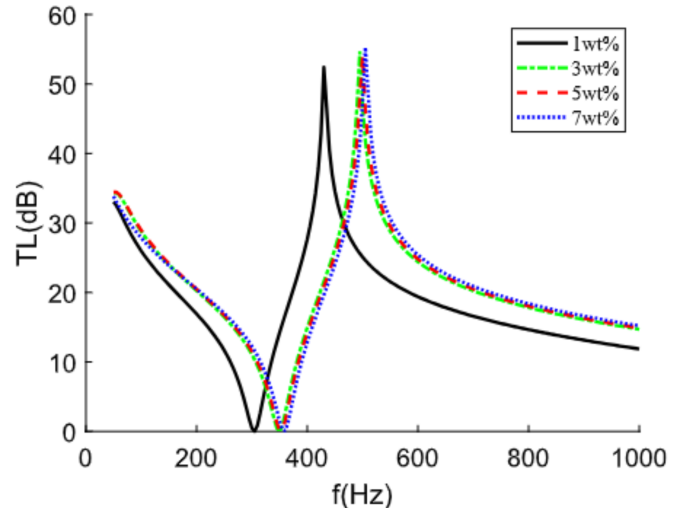


图 10. 碳纳米颗粒质量分数变化对粒子增强 EPDM/ETFE MAM 声传输损失的影响。

与之相比。通过 MD 计算得到的机械参数如表 3 所示，隔音结果如图 10 所示。

在图 10 中，随着碳纳米颗粒的质量分数增加，平均声传输损失增加，声隔离峰值和谷值所在频率向更高频率移动。在不考虑声传输损失曲线移位效应的情况下，还可以注意到，碳纳米颗粒质量分数增加后，600 赫兹后声传输损失曲线的振幅增强。相比之下，3 wt%、5 wt% 和 7 wt% 颗粒增强 MAM 的声传输损失曲线仅因其机械性能的微小变化而略微移位（如表 3 所示）。同时，从表中可以看出，薄膜密度对声隔离曲线性能的影响最大（1 wt% 和 3 wt% 变化最大），而杨氏模量和泊松比在达到一定值后对声隔离峰值频率的影响很小（如 5 wt% 和 7 wt% 曲线所示）。

但声传输损失的衰减速度相对较快；随着 ETFE 比例的增加，传输损失幅度略有下降。因此，通过合理增加 ETFE 材料中 EPDM 的组成比例来提高结构的声学性能是一种有效的方法。

5.2.2. 厚度变化规则 对于颗粒增强的 EPDM/ETFE 薄膜超材料，薄膜厚度称为基底高度 h 。建立了 $h=(0.020, 0.025, 0.030)$ 毫米的理论模型，并分析了相应的声传输损失特性。结果如图 12 所示。从图表中可以看出，增加基底高度不仅增加了结构的平均隔音尺寸，还将隔音峰值向更高频率方向移动。因此，这可以是一种调整隔音频带的常规方法，因为全局局部共振频率的变化以及声波传播路径的变化。

5.2.3. 边长的规律模式 单元边长的变化将改变整体超材料的尺寸，导致声传输损失的变化。将边长从 20 毫米增加到 30 毫米，间隔为 5 毫米。首先建立相应的理论模型，然后计算声传输损失。预测结果如图 13 所示。

如图 13 所示，随着侧长的增加，隔音峰值向低频移动，但随着单元尺寸的增加，宽频带的隔音效果减弱。这是因为以质心位置表示的集中质量在单元中最大。离质心越远，振动越大，使声音更容易传播，传输损失越严重。

5.2. 聚合物固体薄膜的影响

5.2.1. 材料组成对影响趋势 不同材料在复合材料中的比例通常决定了材料的宏观力学性质。基于分子动力学，建立了三个随着 ETFE/EPDM 比例增加的理论模型。复合材料每个理论模型的力学参数见表 4，声传输损失特性见图 11。

可以从这五条曲线看出，随着复合薄膜中 EPDM 比例的增加，隔音的峰值和谷值向低频移动

表 3
具有不同质量分数碳纳米颗粒的材料的机械参数。

弹性特性	碳纳米颗粒			
	1 wt%	3 wt%	5 wt%	7 wt%
杨氏模量, E (GPa)	1.1636	1.4948	1.8244	2.4093
泊松比 (ν)	0.34	0.40	0.43	0.44
密度, ρ	1346	1354	1356	1362

Table 4

Table of mechanical parameters of thin films with different material mass ratios.

Elastic properties	Material Proportion (EPDM:ETFE)				
Young's modulus, E(GPa)	9: 1	7: 3	5:5	3: 7	1: 9
Poisson's ratio (ν)	0.45	0.43	0.42	0.34	0.32
Density, $\rho(\text{kg/m}^3)$	929.7	1034	1172	1346	1592

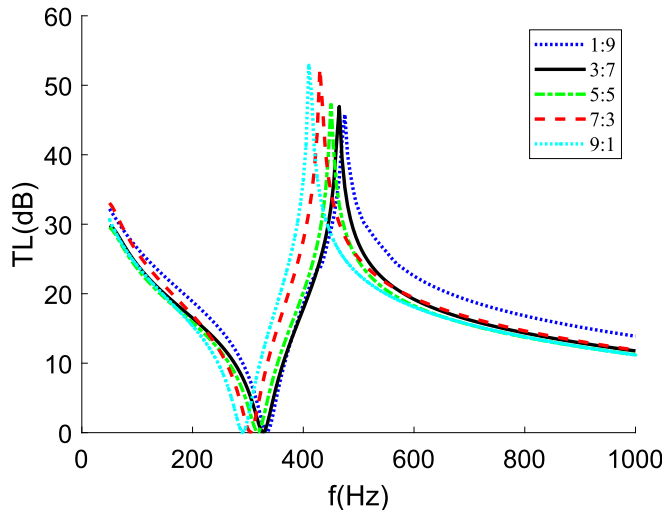


Fig. 11. The law of sound transmission loss changing with the increase of ETFE ratio.

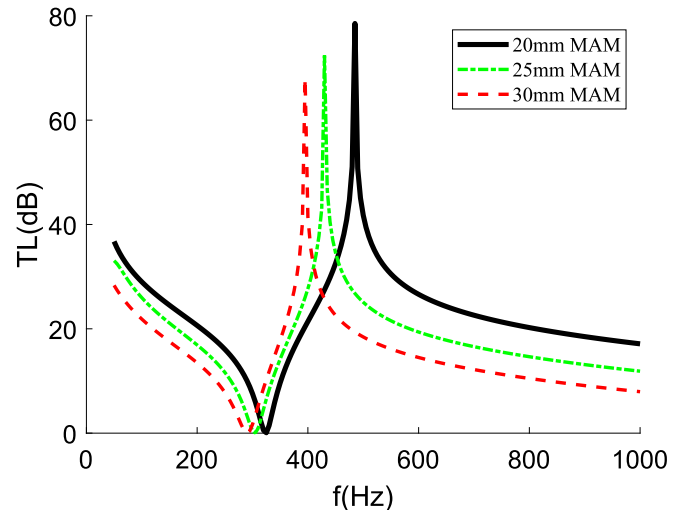


Fig. 13. Sound transmission loss of particle reinforced EPDM/ETFE membrane-type acoustic metamaterials varies with film side length.

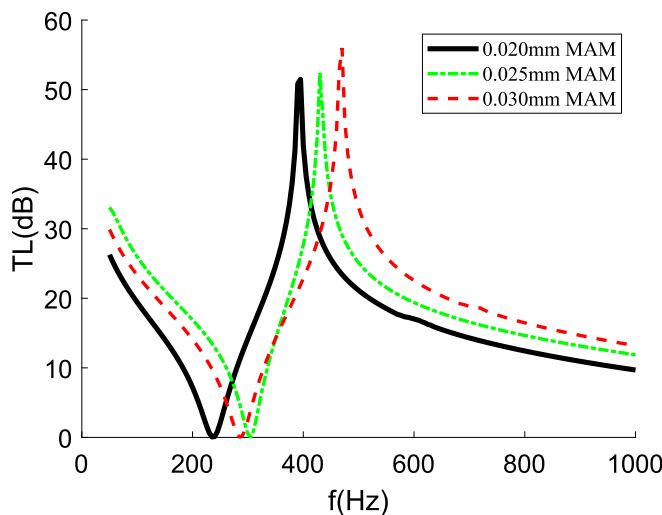


Fig. 12. Sound transmission loss of particle reinforced polymer film evolve with substrate height.

effect. Therefore, the reasonable selection of cell size is necessary for this polymer film metamaterial.

5.3. Affecting rules of mass block

5.3.1. Regulation of mass block thickness variation

For the mass block of particle-reinforced EPDM/ETFE film metamaterial, a theoretical model with height (1, 2, 3) mm was estab-

lished and the corresponding sound transmission loss characteristic law was analysed, the results of which are shown in Fig. 14.

It can be seen from Fig. 14 that the influence of mass block height on its sound transmission loss is quite different from that of base height. The height of the mass block actually affects the area density of the area where the mass block is located. The lower the height of the mass block is, the smaller the area density is. The

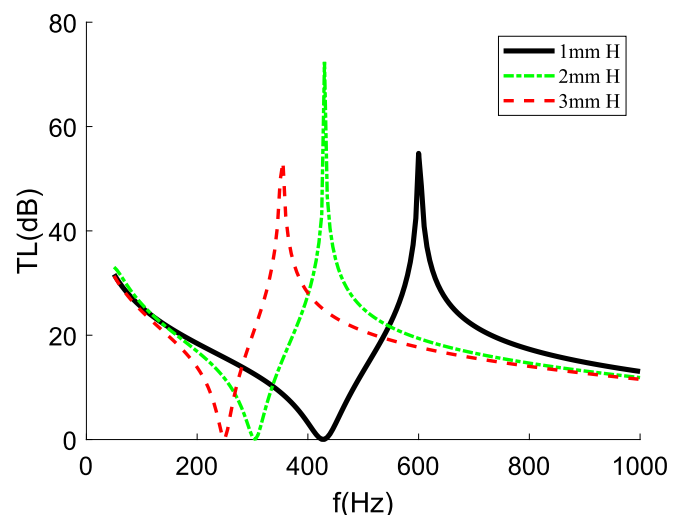


Fig. 14. Sound transmission loss of particle reinforced EPDM/ETFE MAM varies with mass block height.

表4

不同材料质量比的薄膜机械参数表。

弹性特性	材料比例 (EPDM:ETFE)				
	9:1	7:3	5:5	3:7	1:9
杨氏模量, E (GPa)	0.2382	0.3293	0.5507	1.1636	1.2476
泊松比 (ν)	0.45	0.43	0.42	0.34	0.32
密度, q	929.7	1034	1172	1346	1592

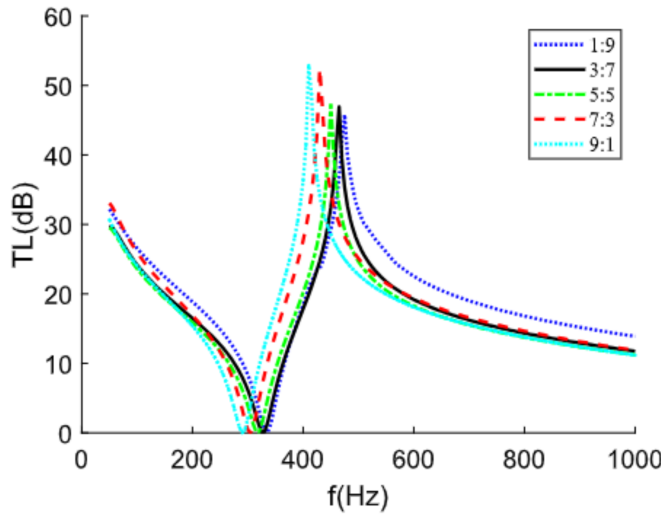


图 11. 随着 ETFE 比例增加, 声传输损失规律的变化。

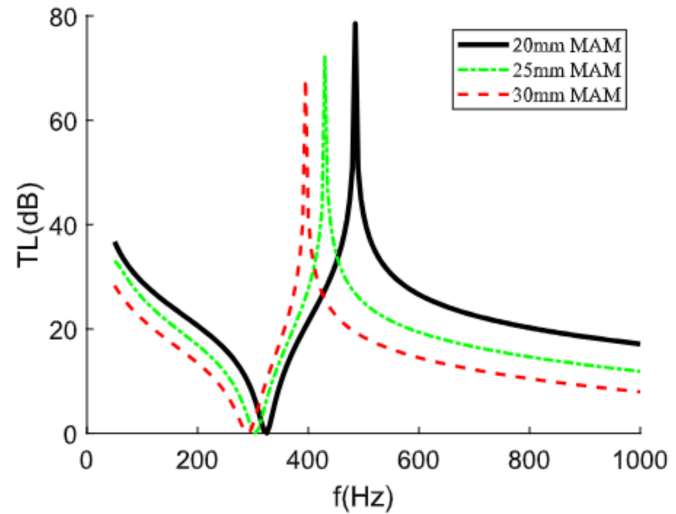


图 13. 颗粒增强 EPDM/ETFE 膜型声学超材料的声传输损失随膜侧长度变化。

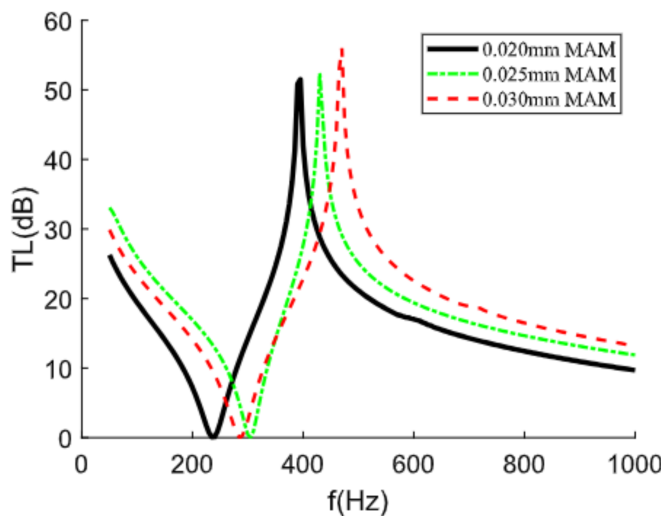


图 12. 颗粒增强聚合物薄膜的声传输损失随基底高度的演变。

因此, 对于这种聚合物薄膜超材料, 合理选择单元尺寸是必要的。

5.3. 影响大块规则

5.3.1. 质量块厚度变化的调节 对于颗粒增强的 EPDM/ETFE 薄膜超材料的质量块, 建立了一个具有高度 (1、2、3) mm 的理论模型。

已发表, 并分析了相应的声传输损失特性规律, 结果如图 14 所示。

从图 14 可以看出, 质量块高度对其声传输损失的影响与基座高度的影响有很大不同。质量块的高度实际上影响了质量块所在区域的面积密度。质量块的高度越低, 面积密度就越小。

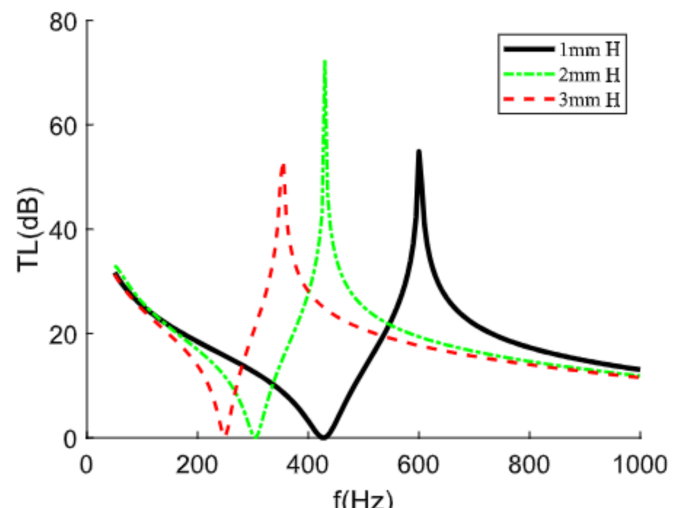


图 14. 颗粒增强 EPDM/ETFE MAM 的声传输损失随质量块高度变化。

sound insulation peak moves to high frequency, and the rising and falling trends are slower than the trend of high thickness. Fig. 15 can explain this phenomenon: different surface vibration velocities lead to different amplitudes of their sound insulation. the highest vibration velocity is at 1 mm height, with a level of 10^{-5} m/s; the minimum at 2 mm is 10^{-8} m/s; and the velocity at 3 mm is 10^{-5} m/s, with a maximum vibration velocity of 10^{-4} m/s. Thus, the peak sound insulation at 2 mm is the largest, and the peak at 3 mm is slightly lower than the peak at 1 mm.

5.3.2. Variation tendency with bottom area

The area density will affect the acoustic transmission loss characteristics of the structure, and the most important factor affecting the surface area density of the structural film is the size of the bottom area of the mass block. Therefore, theoretical models of different cylindrical mass blocks with radius of (1,2,3) mm have been constructed, and their acoustic transmission loss curves are shown in Fig. 16.

From these three curves, it can be seen that the change of area density will not only affect the change of sound insulation peak value, but also change the average sound insulation of the structure. Because this change includes the size of large mass area and the range of high area density area, it is difficult to estimate the optimal frequency range of sound insulation by adjusting the

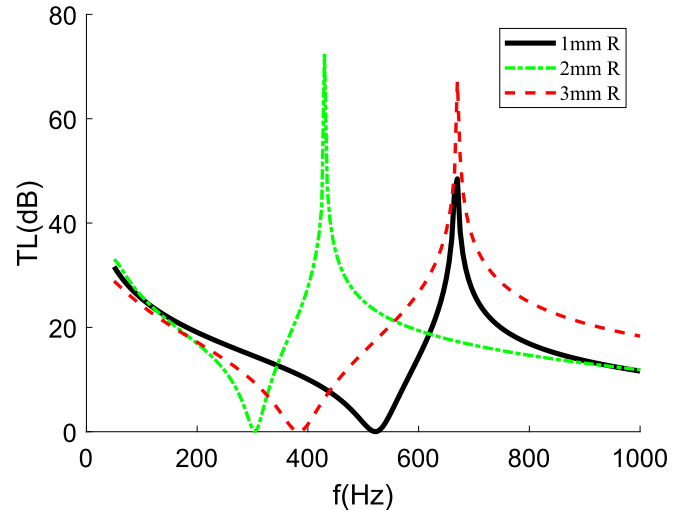


Fig. 16. The sound transmission loss of particle reinforced EPDM/ETFE MAM varies with the bottom area of the mass block.

bottom area of the mass block, but the average sound insulation size of particle reinforced EPDM/ETFE MAM can be effectively improved by increasing the area of the mass block.

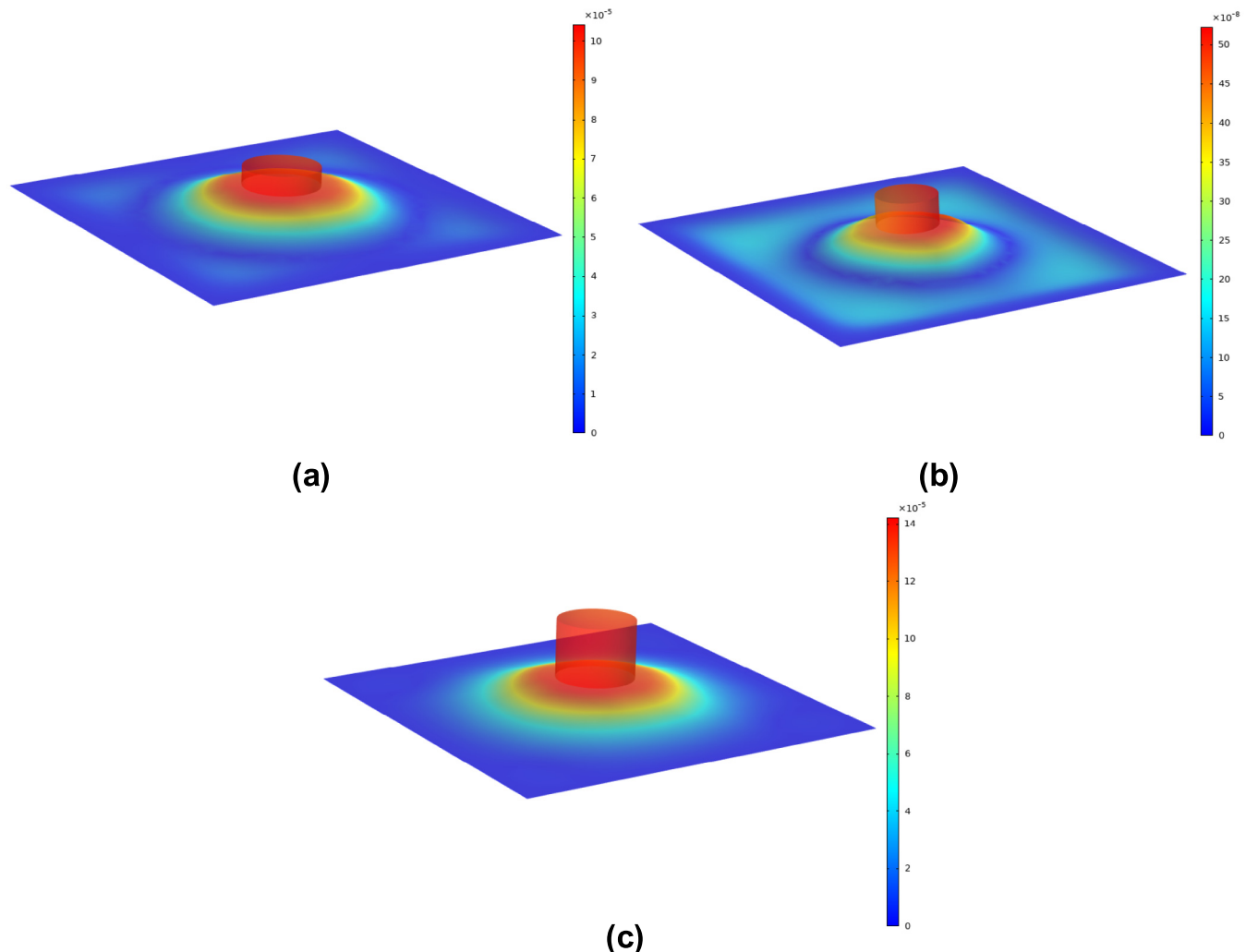


Fig. 15. Peak surface velocity at different heights (a) 1 mm (b) 2 mm (c) 3 mm.

隔音峰值移动到高频，上升和下降趋势比高厚度的趋势慢。图 15 可以解释这种现象：不同表面振动速度导致其隔音幅度不同。最高振动速度在 1 毫米高度，为 10m/s；2 毫米处的最小值为 10m/s；3 毫米处的速度为 10m/s，最大振动速度为 10m/s。因此，2 毫米处的峰值隔音最大，而 3 毫米处的峰值略低于 1 毫米处的峰值。

5.3.2. 底部面积变化趋势 区域密度将影响结构的声传输损失特性，影响结构薄膜表面积密度最重要的因素是质量块底部面积的大小。因此，已构建了不同半径（1、2、3）mm 的圆柱形质量块的理论模型，并在图 16 中显示了它们的声传输损失曲线。

从这三条曲线可以看出，面积密度的变化不仅会影响隔声峰值的变化，还会改变结构的平均隔声。因为这种变化包括大质量区域的大小和高面积密度区域的范围。

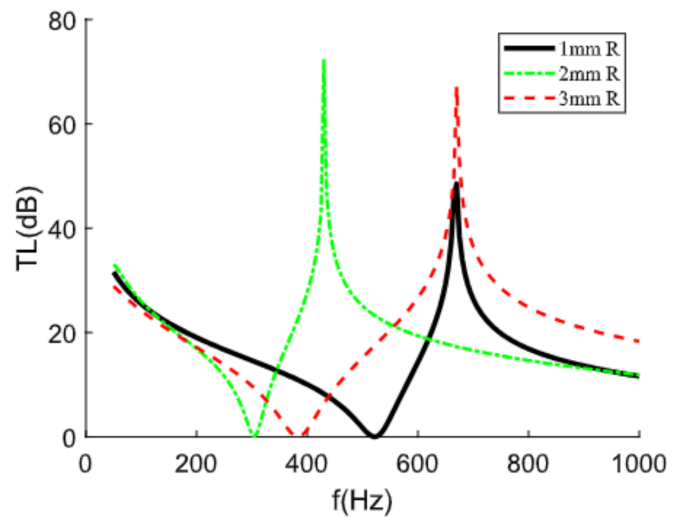


图 16. 颗粒增强的 EPDM/ETFE MAM 的声传输损失随质量块底部面积变化。

通过调整质量块的底部面积来估计声隔离的最佳频率范围是困难的，但通过增加质量块的面积，可以有效提高颗粒增强的 EPDM/ETFE MAM

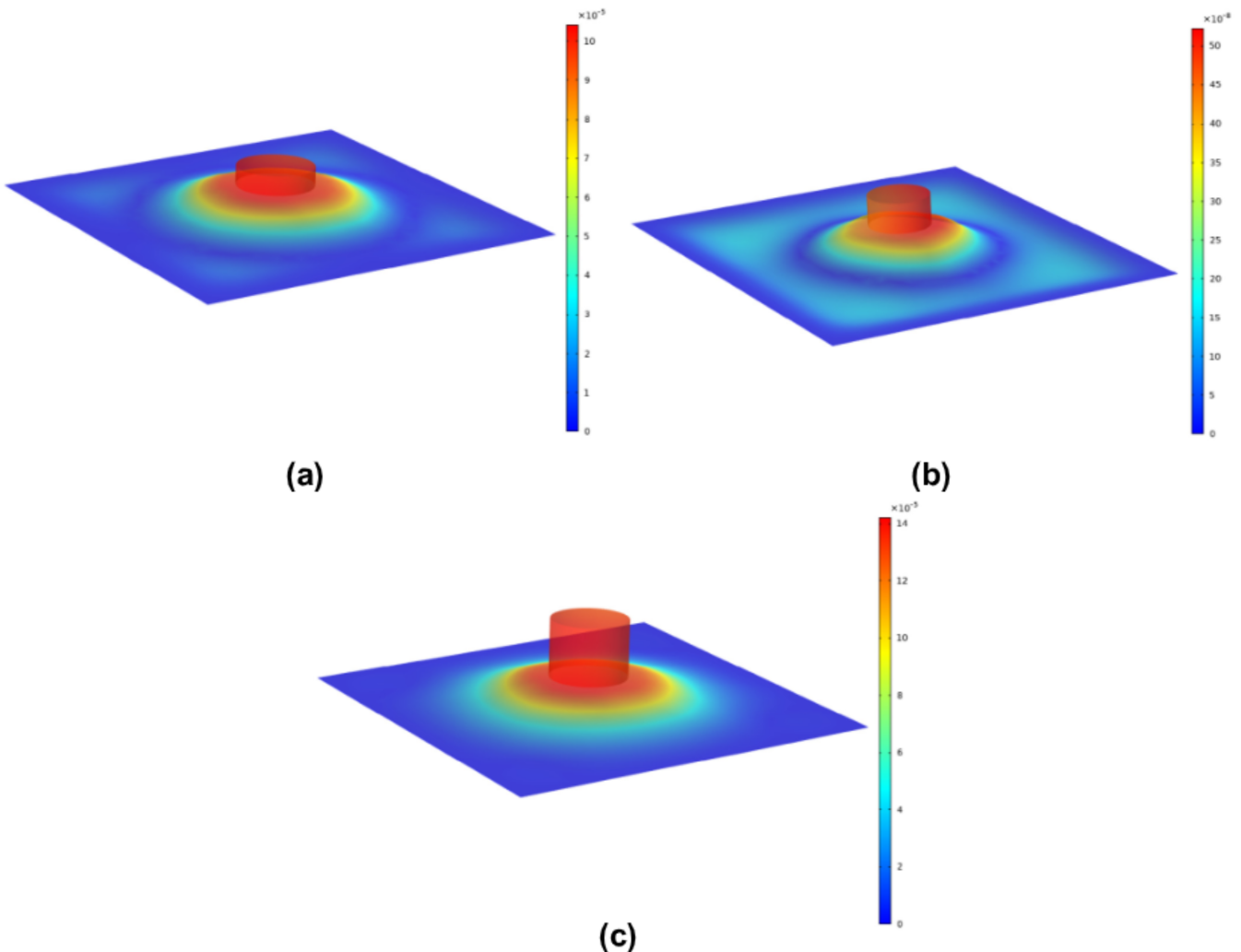


图 15. 不同高度处的峰值表面速度 (a) 1 毫米 (b) 2 毫米 (c) 3 毫米。

Similarly, the surface vibration velocity can explain this phenomenon, as shown in Fig. 17. It can be seen from the figure that the surface vibration velocity with a radius of 1 mm is the largest, and the magnitude reaches 10^{-5} m/s, while the surface vibration velocity with a radius of 2 mm is slightly higher than that with a radius of 3 mm, which leads to the amplitude difference.

The fundamental reason we think is that in addition to the local resonance formed by the mass block-membrane, the modal vibration of the membrane itself will also affect the amplitude of sound insulation, and the mass with different structural dimensions will lead to changes in the vibration characteristics of the membrane.

5.3.3. Effect rule of shape parameter

For the mass blocks with the same volume and different structural shapes, their sound transmission characteristic curves will also change. Here we discuss the influence of cylinders, hollow cylinders, partially hollow cylinders (eccentric 1 mm, eccentric 0.5 mm) and rectangular mass blocks on the structural sound transmission loss, and call them Type 1-Type 5, as shown in Fig. 18.

As can be seen in Fig. 18, the biggest difference between hollow and solid cylinders is that there will be an extra peak of sound

insulation, this is because the hollowing of the mass block changes the distribution of the modal frequencies and vibration patterns of the film, prompting the appearance of multiple frequencies with infinitely small surface vibrations, increasing the number of peaks of sound insulation. The change in the shape of the structure, on the other hand, changes the distribution of the surface density in different areas of the film, which affects the frequency of the peak sound transmission loss and the average size of the sound insulation.

It can be seen from Table 5 that all modes of Type 2 are greater than Type 1, and the sound transmission loss curve is shifted to high frequency as a whole. The first three order modal frequencies of Type 2–4 are very close, which leads to the nearly consistent sound transmission loss characteristics in the early stage. One of the main reasons for the difference in sound insulation between 400 and 600 Hz is the difference in the fourth, fifth and sixth order frequencies. In addition, the centroid eccentricity of Type 3 and Type 4 leads to the change of vibration mode, so that there is another sound insulation fluctuation within 700–800 Hz. The main reason why the sound transmission loss curve of Type 5 differs from other structures is that the modal frequencies of Type 5 differ greatly from other structures.

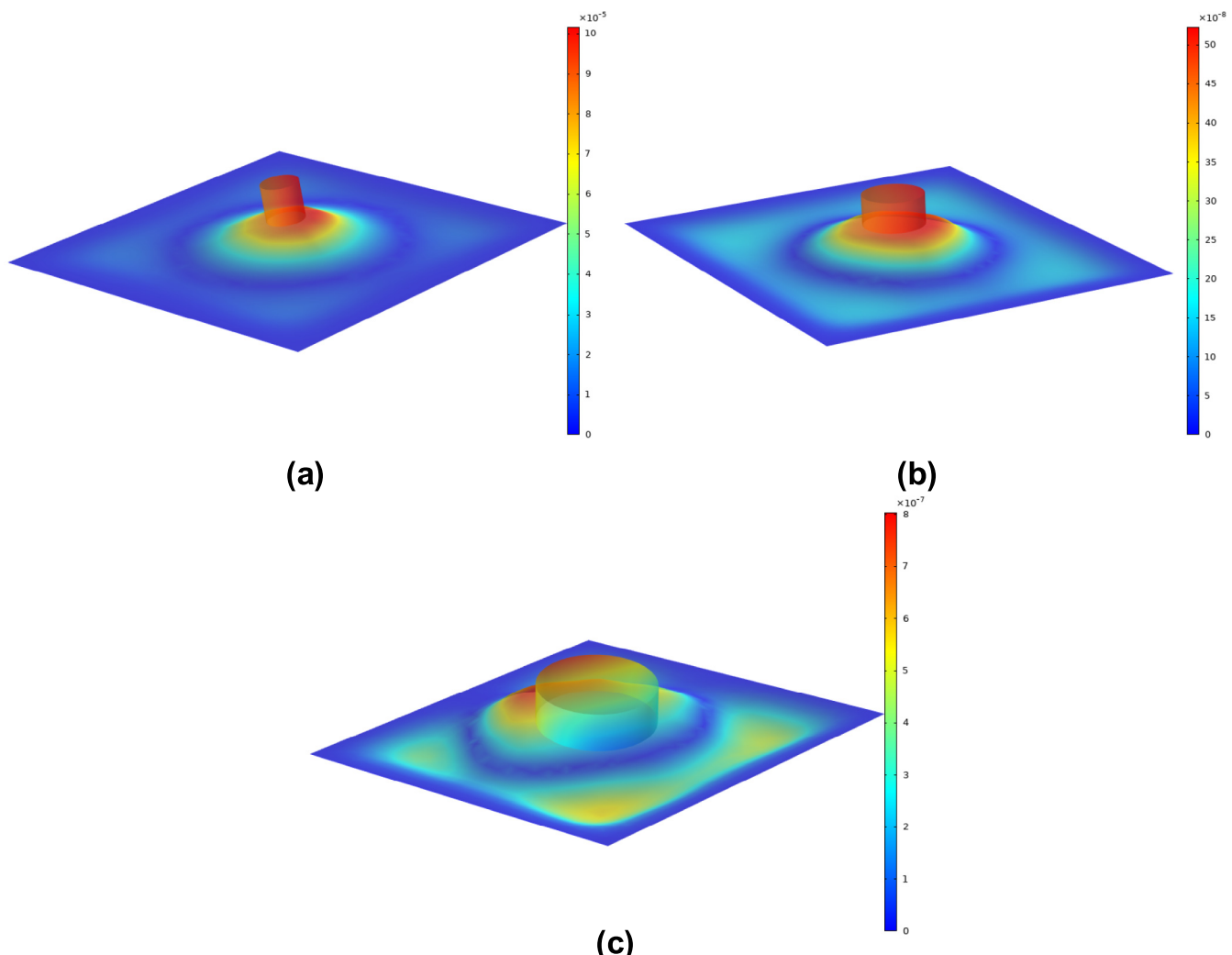


Fig. 17. Peak surface velocity at different radius (a) 1 mm (b) 2 mm (c) 3 mm.

同样，表面振动速度可以解释这一现象，如图 17 所示。从图中可以看出，半径为 1 毫米的表面振动速度最大，幅度达到 10 米/秒，而半径为 2 毫米的表面振动速度略高于半径为 3 毫米的表面振动速度，这导致了振幅差异。

我们认为的根本原因是，除了由质量块-膜形成的局部共振外，膜本身的模态振动也会影响隔音的振幅，而具有不同结构尺寸的质量会导致膜的振动特性发生变化。

5.3.3. 形状参数的影响规则 对于具有相同体积但不同结构形状的质量块，它们的声传输特性曲线也会发生变化。在这里，我们讨论圆柱体、空心圆柱体、部分空心圆柱体（偏心 1 毫米、偏心 0.5 毫米）和矩形质量块对结构声传输损失的影响，并将它们称为类型 1 至类型 5，如图 18 所示。

正如图 18 所示，空心和实心圆柱之间最大的区别在于会有额外的声音峰值。

绝缘，这是因为质量块的空心化改变了薄膜的模态频率和振动模式的分布，促使出现具有无限小表面振动的多频率，增加了隔音峰值的数量。另一方面，结构形状的改变改变了薄膜不同区域的表面密度分布，影响了峰值声传输损失的频率和隔音的平均大小。

从表 5 可以看出，类型 2 的所有模式均大于类型 1，并且整体上声传输损失曲线向高频移动。类型 2-4 的前三阶模态频率非常接近，这导致了早期几乎一致的声传输损失特性。400 和 600 赫兹之间隔音差异的主要原因之一是第四、第五和第六阶频率的差异。此外，类型 3 和类型 4 的质心偏心导致振动模式的变化，从而在 700-800 赫兹范围内出现另一种隔音波动。类型 5 的声传输损失曲线与其他结构不同的主要原因是类型 5 的模态频率与其他结构差异很大。

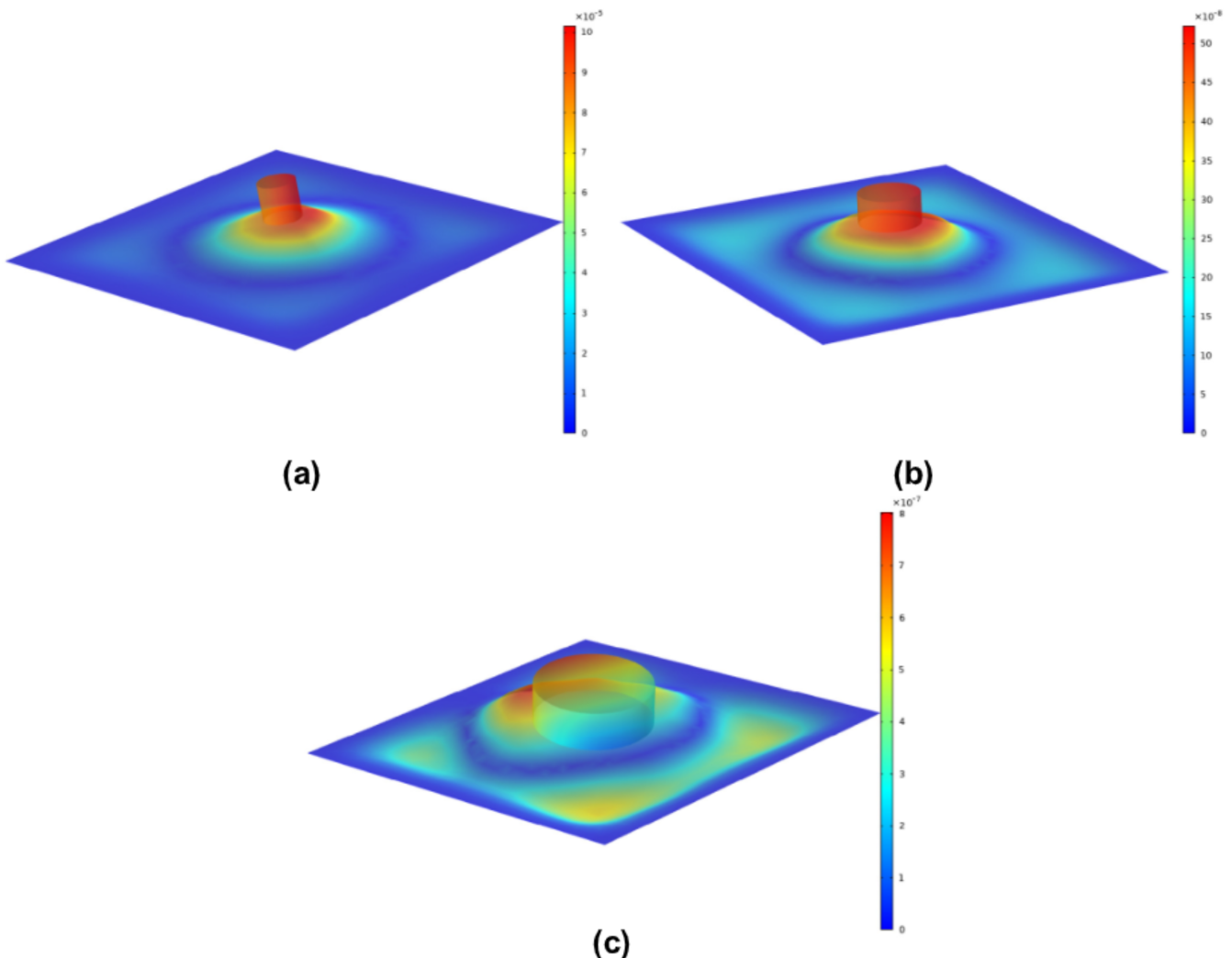


图 17. 不同半径处的峰值表面速度 (a) 1 毫米 (b) 2 毫米 (c) 3 毫米。

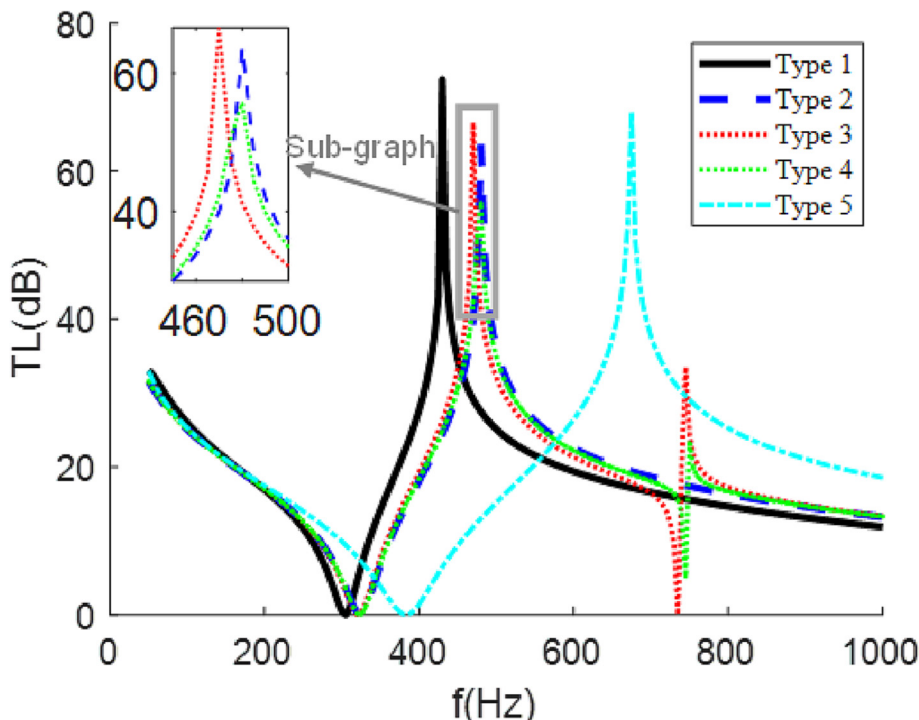


Fig. 18. Variation of sound transmission loss of particle reinforced EPDM/ETFE MAM with mass block shape.

Table 5

The first ten modes of particle reinforced EPDM/ETFE MAM with different masses.

Modal	Type 1	Type 2	Type 3	Type 4	Type 5
1	14.58 Hz	17.94 Hz	17.10 Hz	18.01 Hz	14.58 Hz
2	54.33 Hz	60.84 Hz	58.37 Hz	56.57 Hz	59.86 Hz
3	57.60 Hz	63.69 Hz	68.56 Hz	66.38 Hz	59.90 Hz
4	357.99 Hz	460.28 Hz	417.57 Hz	448.43 Hz	377.23 Hz
5	376.43 Hz	499.69 Hz	465.21 Hz	465.63 Hz	423.89 Hz
6	420.65 Hz	538.09 Hz	491.72 Hz	538.90 Hz	424.01 Hz
7	493.68 Hz	652.01 Hz	588.52 Hz	616.26 Hz	492.76 Hz
8	540.29 Hz	668.61 Hz	629.21 Hz	638.18 Hz	780.90 Hz
9	731.40 Hz	882.91 Hz	804.63 Hz	837.39 Hz	1017.7 Hz
10	773.07 Hz	958.95 Hz	847.85 Hz	942.85 Hz	1018.1 Hz

6. Conclusion

This paper proposes a particle-reinforced polymer film metamaterial for the poor acoustic performance of ETFE membrane structure buildings, focusing on the structural sound insulation potential in the low frequency range where sound is not easily controlled. The base film of the structure consists of a composite of EPDM and ETFE with excellent acoustic properties, and the introduction of carbon nanoparticles that improve the mechanical properties. The overall structure is composed of a large mass of regular metal blocks loaded on the film. The first part of this work is to develop the macroscopic mechanical properties of the composite polymer material using MS software; secondly to construct a complete three-dimensional sound transmission loss prediction model of a polymer thin film acoustic metamaterial using the idea of discrete point matching. At the same time, based on COMSOL Multiphysics 5.6 software, the acoustic structure coupling finite element model of the particle reinforced EPDM/ETFE MAM was established, and the transmission loss characteristics were analyzed, which verified the accuracy and reliability of the above

methods, and also confirmed the superiority of the structure in low-frequency sound insulation. The potential of this structure for ETFE membrane construction is further demonstrated by comparing the sound transmission loss of this structure with that of an equivalent mass polymer membrane structure and a metal membrane structure. Finally, the influence law of 7 kinds of influencing factors, including mass fraction of carbon nanoparticles and physical parameters of EPDM/ETFE materials, on the sound insulation properties of this particle-reinforced polymer film metamaterial is discussed in depth, with the following main conclusions.

- 1) The sound transmission properties of this MAM are mainly formed by the local resonance of the structure and the regional surface density resulting in different frequencies and amplitudes of the structural vibration modes, and different magnitudes of surface vibrations.
- 2) This particle-reinforced polymer thin film metamaterial differs from simple membrane and plate structures in that it can effectively improve the sound insulation of thin film buildings in some of the lower frequency bands. The struc-

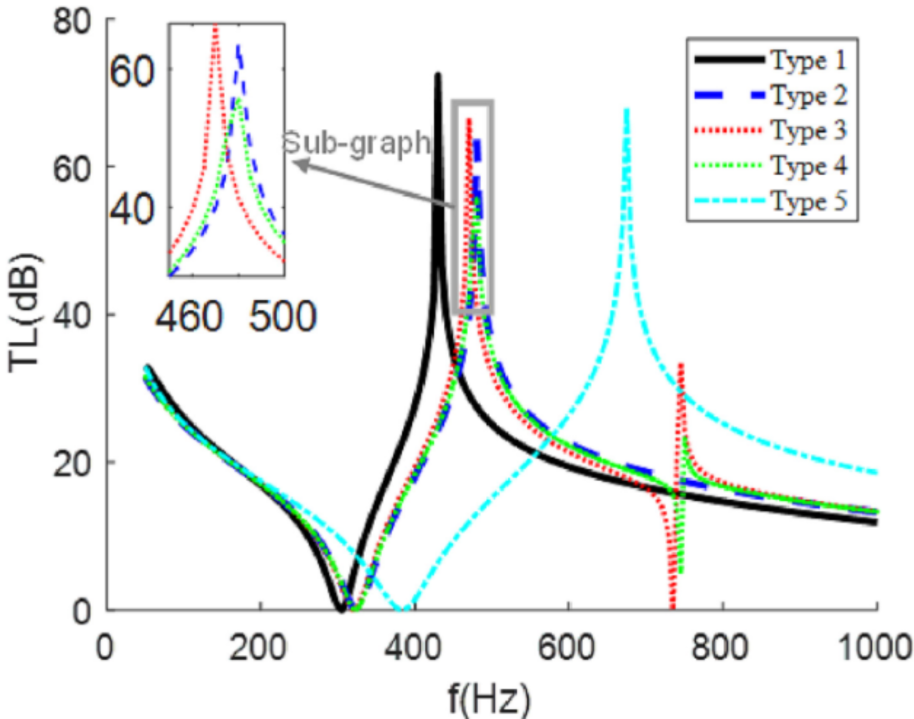


图 18. 带有质量块形状的颗粒增强 EPDM/ETFE MAM 声传输损失变化。

表 5

粒子增强的 EPDM/ETFE MAM 的前十种模式，具有不同的质量。

模态	类型 1	类型 2	类型 3	类型 4	类型 5
1	14.58 赫兹	17.94 赫兹	17.10 赫兹	18.01 赫兹	14.58 赫兹
2	54.33 赫兹	60.84 赫兹	58.37 赫兹	56.57 赫兹	59.86 赫兹
3	57.60 赫兹	63.69 赫兹	68.56 赫兹	66.38 赫兹	59.90 赫兹
4	357.99 赫兹	460.28 赫兹	417.57 赫兹	448.43 赫兹	377.23 赫兹
5	376.43 赫兹	499.69 Hz	465.21 Hz	465.63 Hz	423.89 Hz
6	420.65 Hz	538.09 赫兹	491.72 赫兹	538.90 赫兹	424.01 赫兹
7	493.68 赫兹	652.01 赫兹	588.52 赫兹	616.26 赫兹	492.76 赫兹
8	540.29 赫兹	668.61 赫兹	629.21 赫兹	638.18 赫兹	780.90 赫兹
9	731.40 赫兹	882.91 Hz	804.63 Hz	837.39 Hz	1017.7 Hz
10	773.07 Hz	958.95 Hz	847.85 Hz	942.85 Hz	1018.1 Hz

6. 结论 本文提出了一种用于改善 ETFE 膜结构建筑声学性能的颗粒增强聚合物薄膜超材料，重点关注声音在低频范围内的结构隔音潜力，这是声音不容易控制的范围。结构的基膜由具有优异声学性能的 EPDM 和 ETFE 复合材料组成，并引入了改善机械性能的碳纳米颗粒。整体结构由大量常规金属块组成，加载在薄膜上。这项工作的第一部分是利用 MS 软件开发复合聚合物材料的宏观力学性能；其次，利用离散点匹配的思想构建了聚合物薄膜声学超材料的完整三维声传输损失预测模型。同时，基于 COMSOL Multiphysics 5.6 软件，建立了颗粒增强 EPDM/ETFE MAM 的声学结构耦合有限元模型，并分析了传输损失特性。

验证了上述方法的准确性和可靠性，并确认了该结构在低频隔音方面的优越性。通过比较该结构的声传输损失与等质量聚合物膜结构和金属膜结构的声传输损失，进一步展示了该结构在 ETFE 膜建筑中的潜力。最后，深入讨论了碳纳米颗粒质量分数和 EPDM/ETFE 材料物理参数等 7 种影响因素对这种颗粒增强聚合物薄膜超材料隔音性能的影响规律，并得出以下主要结论。

- 1) 这种 MAM 的声传输特性主要由结构的局部共振和区域表面密度形成，导致结构振动模式的不同频率和振幅，以及表面振动的不同幅度。
- 2) 这种颗粒增强聚合物薄膜超材料与简单的膜和板结构不同，它可以有效地提高一些较低频段的薄膜建筑的隔音性能。

ture shown in this paper can achieve sound insulation levels of up to 60 dB near 0.5 kHz and outperforms purely equal-mass film structures throughout the low frequency range (50 Hz – 1000 Hz).

- 3) It can be seen from the influence factors deeply studied in this paper that proper adjustment of structural physical parameters can change the frequency of the sound insulation peak value, making it possible to improve the sound insulation for the characteristic frequency.

However, from all the work in this paper it can be found that large sound insulation over a wide frequency band is still not easy to achieve. Of course, for the multi-layer membrane composition that is now common in ETFE membrane buildings, it is possible to consider selecting a multi-layer supermaterial series-parallel structure composed of different material parameters and structural parameters to improve its broadband sound transmission losses. Therefore, in future work, we will study the sound transmission loss characteristics law of this particle-reinforced EPDM/ETFE film metamaterial in series and parallel with multiple cell elements and multiple sizes, with the goal of further enhancing the effective frequency band of large sound insulation (frequency band range > 200 Hz at low frequencies and sound insulation > 30 dB).

Data availability

The data used to support the findings of this study are available from the corresponding author upon request.

CRediT authorship contribution statement

Junyu Li: Conceptualization, Methodology, Software, Writing – original draft, Data curation. **Renjie Jiang:** Validation, Writing – review & editing, Software. **Di Xu:** Investigation, Resources. **Qibai Huang:** Conceptualization, Writing – review & editing, Supervision, Funding acquisition.

Data availability

Data will be made available on request.

Declaration of Competing Interest

The authors declare the following financial interests/personal relationships which may be considered as potential competing interests: Qibai Huang reports financial support was provided by Guangxi Science and Technology Major Project.

Acknowledgments

This work is supported by Guangxi Science and Technology Major Project (Gui Science AA22068060-6). The author is very grateful for these supports.

References

- [1] Bing Zhao, Leiting Dong, Wujun Chen, Jianhui Hu, Zhenyu Qiu, Jinyu Zhou, Mechanical properties and structural performance of ETFE (ethylene-tetrafluoroethylene) cushion structures at low temperatures, Eng Struct, Volume 136, 2017, Pages 420-429, ISSN 0141-0296, <https://doi.org/10.1016/j.engstruct.2017.01.031>.
- [2] Gao C, Lu M, Lu H, et al. Application Research of ETFE Membrane in the Metro Entrance Design[J]. Constr Technol 2015.
- [3] J. Hu, W. Chen, B. Zhao, D. Yang. Buildings with ETFE foils: a review on material properties, architectural performance and structural behavior Constr Build Mater, 131 (2017), pp. 411-422.
- [4] Paech C. Structural membranes used in modern building facades. Procedia Eng 2016;155:61–70.
- [5] Jia LX, Wang DW. Study on Application of Membrane Structure in the Sports Building. AMM 2014;638–640:295–9. <https://doi.org/10.4028/www.scientific.net/amm.638-640.295>.
- [6] Huang H, Li X, Xue S, Luo Y, Shi D, Hou X, et al. Performance and Measurement Devices for Membrane Buildings in Civil Engineering: A Review. Appl Sci 2022;12(17):8648. <https://doi.org/10.3390/app12178648>.
- [7] Gallio C, Luchsinger RH. Uniaxial and biaxial mechanical properties of ETFE foils. Polym Test 2011;30:356–65.
- [8] Charbonneau L, Polak MA, Penlidis A. Mechanical properties of ETFE foils: testing and modelling. Constr Build Mater 2014;60:63–72.
- [9] Hu J, Chen W, Luo R, Zhao B, Sun R. Uniaxial cyclic tensile mechanical properties of ethylene tetrafluoroethylene (ETFE) foils. Constr Build Mater 2014;63:311–9.
- [10] Hu J, Chen W, Zhao B, Wang K. Uniaxial tensile mechanical properties and model parameters determination of ethylene tetrafluoroethylene (ETFE) foils. Constr Build Mater 2015;75:200–7.
- [11] Sheng JR, Zhang TJ. Research on Light-Duty and Energy-Saving Characteristic of Membrane Structure and its Development Prospect. AMR 2011;250–253:925–30. <https://doi.org/10.4028/www.scientific.net/amr.250-253.925>.
- [12] Poirazis H, Kragn M, Hogg C. Energy modelling of ETFE membranes in building applications. In: Proceedings of the eleventh international IBPSA conference on building simulation. Glasgow, Scotland; July 27–30 2009.
- [13] Mainini AG, Poli T, Paolini R, Zinzi M, Vercesi L. Transparent multilayer ETFE panels for building envelope: thermal transmittance evaluation and assessment of optical and solar performance decay due to soiling. Energy Procedia 2014;48:1302–10.
- [14] Mainini AG, Speroni A, Zani A, Poli T. The effect of water spray systems on thermal and solar performance of an ETFE panel for building envelope. Procedia Eng 2016;155:352–60.
- [15] Ahadi M, Andisheh-Tadbir M, Tam M, Bahrami M. An improved transient plane source method for measuring thermal conductivity of thin films: deconvoluting thermal contact resistance. Int J Heat Mass Transf 2016;96:371–80.
- [16] Robinson-Gayle S, Kolokotroni M, Cripps A, Tanno S. ETFE foil cushions in roofs and atria. Constr Build Mater 2001;15:323–7.
- [17] Candemir KU. Inflatable pillow system as a glass substitute in terms of building envelope [M.Sc. thesis]. Turkey: Izmir Institute of Technology; 2003.
- [18] Cremers J. Environmental impact of membrane and foil materials and structures –status quo and future outlook. Technical transactions. Architecture. 7-A; 2014.
- [19] Monticelli C, Campioli A, Zanelli A. Environmental load of ETFE cushions and future ways for their self-sufficient performances. In: Domingo Alberto, Lazaro Carlos, editors. Proceedings of the International Association for Shell and Spatial Structures (IASS) Symposium 2009, Valencia, Evolution and Trends in Design, Analysis and Construction of Shell and Spatial Structures. 28 September – 2 October 2009, Universidad Politecnica de Valencia, Spain.
- [20] Maywald C, Riesser F. Sustainability – the art of modern architecture. Proc Eng 2016;155:238–48. <https://doi.org/10.1016/j.proeng.2016.08.025>.
- [21] Franta P. Applying Double Skin Façade with ETFE Membrane Assembly for Energy Saving and Acoustic Protection for the Building of the Czech Institute of Informatics, Robotics and Cybernetics in Prague. J Civil Eng Archit 2019.
- [22] Zhao X, Long ES, Huang LH. Design Measures of Low Carbon Buildings with Exterior Envelope Made of ETFE Air Pillows. AMR 2010;168–170:2524–8. <https://doi.org/10.4028/www.scientific.net/amr.168-170.2524>.
- [23] Chen W. Design of membrane structure engineering [M]. Beijing: China Architecture and Building Press, 2005: 118–140 (in Chinese).
- [24] Jones A, Hamilton D, Purvis M, Jones M. Eden project, Cornwall: design, development and construction. Struct Eng 2001;79:30–6.
- [25] Chen X, Zhao Z, Zhang X. Application of ETFE membrane structure on national aquatics center (Water Cube). Arch Technol 2008;3:006.
- [26] Chiu S, Noble D, Valmont E. 9 – Acoustics in architectural fabric structures: the case of ETFE pillows. In: Fabric structures in architecture, A volume in Woodhead Publishing Series in textiles. Elsevier; 2015. p. 241–56.
- [27] Masahiro Toyoda, Daiji Takahashi, Reduction of rain noise from Ethylene/TetraFluoroEthylene membrane structures, Applied Acoustics, Volume 74, Issue 12, 2013, Pages 1309-1314, ISSN 0003-682X, <https://doi.org/10.1016/j.apacoust.2013.05.013>.
- [28] Toyoda M, Takahashi D. Reduction of rain noise from Ethylene/TetraFluoroEthylene membrane structures. Appl Acoust 2013;74:1309–14. <https://doi.org/10.1016/j.apacoust.2013.05.013>.
- [29] Rychtáříková, Monika, Daniel Urbán, Carl Maywald, Lukáš Zelem, Magdaléna Kaššáková a Christ Glorieux. Advantages of ETFE in terms of acoustic comfort in atria and large halls. 12th Conference on Advanced Building Skins. Wilen (Switzerland): Advanced Building Skins, 2017, 646–654. ISBN 978-3-9524883-1-7.
- [30] Kushal G. Ambli, Bhimanagoud M. Dodamani, Jagadeesh A., Mohan B. Vanarotti, Heterogeneous composites for low and medium temperature thermal insulation: A review, Energy and Buildings, Volume 199, 2019, Pages 455–460, ISSN 0378-7788, <https://doi.org/10.1016/j.enbuild.2019.07.024>.
- [31] Hosseinpour A, Katbab AA, Ohadi A. A novel sound absorber foam based on ethylene propylene diene monomer (EPDM) to absorb low-frequency waves: Influence of EPDM ethylene content. Polym Eng Sci 2022.
- [32] Fei Y, Fang W, Zhong M, Jin J, Fan P, Yang J, et al. Morphological Structure, Rheological Behavior, Mechanical Properties and Sound Insulation Performance of Thermoplastic Rubber Composites Reinforced by Different Inorganic Fillers[J]. Polymers 2018;10(3):276.

本文中所展示的结构可以在 0.5 kHz 附近实现高达 60 dB 的隔音水平，并且在整个低频范围（50 Hz 至 1000 Hz）优于纯等质量薄膜结构。

3) 从本文深入研究的影响因素可以看出，适当调整结构物理参数可以改变隔音峰值的频率，从而可能提高特征频率的隔音效果。

然而，从本文的所有工作中可以发现，要实现在宽频带上的大声音隔绝仍然不容易。当然，对于如今在 ETFE 膜建筑中常见的多层膜组合，可以考虑选择由不同材料参数和结构参数组成的多层次超材料串联结构，以改善其宽带声传输损耗。因此，在未来的工作中，我们将研究这种粒子增强的 EPDM/ETFE 膜超材料在串并联多个单元元件和多个尺寸中的声传输损耗特性规律，旨在进一步增强大声隔绝的有效频带（低频带范围 > 200 Hz，声隔绝 > 30 dB）。

数据可用性

本研究所使用的数据可根据请求从相应作者处获取。

CRediT 作者贡献声明

李俊宇：概念化、方法论、软件、写作-原始草稿、数据整理。姜仁杰：验证、写作-审阅和编辑、软件。徐迪：调查、资源。黄启白：概念化、写作-审阅和编辑、监督、资金获取。

数据可用性

数据将根据请求提供。

利益竞争声明

作者声明以下可能被视为潜在竞争利益的财务利益/个人关系：黄启白报告广西科技重大项目提供了财务支持。

致谢

本工作得到广西科技重大项目（桂科 AA22068060-6）的支持。作者对这些支持表示非常感激。

参考资料

- [1] 赵兵, 董雷霆, 陈武军, 胡建辉, 邱振宇, 周金宇, ETFE (聚四氟乙烯) 垫结构在低温下的力学性能和结构性能, *Eng Struct.*, 卷 136, 2017 年, 页码 420-429, ISSN 0141-0296, <https://doi.org/10.1016/j.engstruct.2017.01.031>. [2] 高超, 陆敏, 陆辉等, ETFE 膜在地铁入口设计中的应用研究[J]. *Constr Technol.* 2015. [3] 胡建辉, 陈武军, 赵兵, 杨丹, ETFE 薄膜建筑: 材料性能、建筑性能和结构行为综述 *Constr Build Mater.*, 131 (2017), 页码 411-422. [4] Paech C. 现代建筑立面中使用的结构膜. *Procedia Eng.* 2016;155:61-70.
- [5] 贾 LX, 王 DW. 膜结构在体育建筑中的应用研究. *AMM* 2014; 638-640: 295-9. <https://doi.org/10.4028/www.scientific.net/amm.638-640.295>.
- [6] 黄华, 李雪, 薛松, 罗勇, 史迪, 侯雪等. 土木工程中膜结构建筑的性能和测量设备: 综述. *Appl Sci* 2022;12(17):8648. <https://doi.org/10.3390/app12178648>. [7] 加利奥特 C, 卢克辛格 RH. ETFE 薄膜的单轴和双轴力学性能. *Polym Test* 2011;30:356 - 65. [8] 夏尔邦诺 L, 波拉克 MA, 彭利迪斯 A. ETFE 薄膜的力学性能: 测试和建模. *Constr Build Mater* 2014;60:63 - 72. [9] 胡杰, 陈伟, 罗瑞, 赵斌, 孙瑞. 乙烯四氟乙烯 (ETFE) 薄膜的单轴循环拉伸力学性能. *Constr Build Mater* 2014;63:311 - 9.
- 胡 J, 陈 W, 赵 B, 王 K. 乙烯四氟乙烯 (ETFE) 薄膜的单轴拉伸力学性能和模型参数确定. *Constr Build Mater* 2015;75:200 - 7.
- [11] 盛 JR, 张 TJ. 轻型和节能特性研究
膜结构及其发展前景. *AMR* 2011;250 - 253:925 - 30. <https://doi.org/10.4028/www.scientific.net/amr.250-253.925>.
- [12] Poirazis H, Kragh M, Hogg C. ETFE 膜在建筑中的能源建模
应用. 在: 建筑模拟第十一届国际 IBPSA 会议论文集. 苏格兰格拉斯哥; 2009 年 7 月 27 日至 30 日.
- [13] Mainini AG, Poli T, Paolini R, Zinzi M, Vercesi L. 透明多层 ETFE
建筑物外围面板: 由于污垢导致光学和太阳性能衰减的热传递评估和评估. *能源程序* 2014 年; 48:1302-10.
- [14] Mainini AG, Speroni A, Zani A, Poli T. 水雾系统对建筑外围 ETFE 板的热性能和太阳能性能的影响.
Procedia Eng 2016;155:352 - 60.
- [15] 阿哈迪 M, 安迪舍-塔德比尔 M, 谭 M, 巴赫拉米 M. 一个改进的瞬态平面
source method for measuring thermal conductivity of thin films:
deconvoluting thermal contact resistance. *Int J Heat Mass Transf* 2016;96:371 - 80.
- [16] Robinson-Gayle S, Kolokotroni M, Cripps A, Tanno S. ETFE foil cushions in
roofs and atria. *Constr Build Mater* 2001;15:323 - 7. [17] Candemir KU.
Inflatable pillow system as a glass substitute in terms of building envelope
[M.Sc. thesis]. Turkey: Izmir Institute of Technology; 2003. [18] Cremers J.
Environmental impact of membrane and foil materials and
structures - status quo and future outlook. *Technical transactions.
Architecture.* 7-A; 2014.
- [19] Monticelli C, Campioli A, Zanelli A. Environmental load of ETFE cushions and
future ways for their self-sufficient performances. In: Domingo Alberto,
Lazaro Carlos, editors. *Proceedings of the International Association for
Shell and Spatial Structures (IASS) Symposium 2009*, Valencia, Evolution
and Trends in Design, Analysis and Construction of Shell and Spatial
Structures. 28 September - 2 October 2009, Universidad Politecnica de
[20] MayandaaC, Späthauer F. Sustainability - the art of modern architecture.
Proc Eng 2016;155:238 - 48. <https://doi.org/10.1016/j.proeng.2016.08.025>. [21]
Franta P. Applying Double Skin Façade with ETFE Membrane Assembly for
Energy Saving and Acoustic Protection for the Building of the Czech
Institute of Informatics, Robotics and Cybernetics in Prague. *J Civil Eng*
[22] Zhabikovc18049ES, Huang LH. Design Measures of Low Carbon Buildings with
Exterior Envelope Made of ETFE Air Pillows. *AMR* 2010;168 - 170:2524 - 8.
<https://doi.org/10.4028/www.scientific.net/amr.168-170.2524>.
- [23] Chen W. Design of membrane structure engineering [M]. Beijing: China
Architecture and Building Press, 2005: 118 - 140 (in Chinese). [24] Jones A,
Hamilton D, Purvis M, Jones M. Eden project, Cornwall: design, development and
construction. *Struct Eng* 2001;79:30 - 6. [25] Chen X, Zhao Z, Zhang X.
Application of ETFE membrane structure on national aquatics center (Water
Cube). *Arch Technol* 2008;3:006. [26] Chiu S, Noble D, Valmont E. 9 - Acoustics
in architectural fabric structures: the
case of ETFE pillows. In: *Fabric structures in architecture, A volume in
Woodhead Publishing Series in textiles*. Elsevier; 2015. p. 241 - 56.
- [27] Masahiro Toyoda, Daiji Takahashi, Reduction of rain noise from Ethylene/
TetraFluoroEthylene membrane structures, *Applied Acoustics*, Volume 74,
Issue 12, 2013, Pages 1309-1314, ISSN 0003-682X,
<https://doi.org/10.1016/j.apacoust.2013.05.016>.
- [28] Toyoda M, Takahashi D. Reduction of rain noise from Ethylene/
TetraFluoroEthylene membrane structures. *Appl Acoust* 2013;74:1309 - 14.
<https://doi.org/10.1016/j.apacoust.2013.05.013>.
- [29] Rychtáříková, Monika, Daniel Urbán, Carl Maywald, Lukáš Zelem, Magdaléna
Kaššáková a Christ Glorieux. Advantages of ETFE in terms of acoustic
comfort in atria and large halls. 12th Conference on Advanced Building
Skins. Wilen (Switzerland): Advanced Building Skins, 2017, 646-654. ISBN
978-3-95248831-7.
- [30] Kushal G, Ambli, Bhimanagoud M, Dodamani, Jagadeesh A., Mohan B, Vanarotti,
Heterogeneous composites for low and medium temperature thermal
insulation: A review, *Energy and Buildings*, Volume 199, 2019, Pages 455-
460, ISSN 0378-7788, <https://doi.org/10.1016/j.enbuild.2019.07.024>.
- [31] Hosseinpour A, Katbab AA, Ohadi A. A novel sound absorber foam based on
ethylene propylene diene monomer (EPDM) to absorb low-frequency waves:
Influence of EPDM ethylene content. *Polym Eng Sci* 2022.
- [32] Fei Y, Fang W, Zhong M, Jin J, Fan P, Yang J, et al. Morphological Structure,
Rheological Behavior, Mechanical Properties and Sound Insulation
Performance of Thermoplastic Rubber Composites Reinforced by Different
Inorganic Fillers[J]. *Polymers* 2018;10(3):276.

- [33] Y Fei, F Chen, W Fang, L Xu, S Ruan, X Liu, M Zhong, T Kuang. High-strength, flexible and cycling-stable piezo-resistive polymeric foams derived from thermoplastic polyurethane and multi-wall carbon nanotubes[J]. Composites Part B: Engineering, accepted.
- [34] Fei Y, Fang W, Zhong M, Jin J, Fan P, Yang J, et al. Extrusion Foaming of Lightweight Polystyrene Composite Foams with Controllable Cellular Structure for Sound Absorption Application[J]. Polymers 2019;11(1):106.
- [35] Fang W, Fei Y, Lu H, Jin J, Zhong M, Fan P, et al. Enhanced sound insulation and mechanical properties based on inorganic fillers/thermoplastic elastomer composites[J]. J Thermoplast Compos Mater 2018;089270571876638.
- [36] Chen S, Zhu W, Cheng Y. Multi-Objective Optimization of Acoustic Performances of Polyurethane Foam Composites. Polymers 2018;10(7):788. <https://doi.org/10.3390/polym10070788>.
- [37] Albooyeh A, Dadras A, Mashhadzadeh AH. Effect of point defects and low-density carbon-doped on mechanical properties of BNNTs: A molecular dynamics study. Mater Chem Phys 2020;239:122107.
- [38] Zhichao Xu, Huang Q. Vibro-acoustic analysis of functionally graded graphene reinforced nanocomposite laminated plates under thermal-mechanical loads [J]. Eng Struct 2019;186:345–55.
- [39] Zhichao Xu, Zhang Z, Wang J, et al. Acoustic analysis of functionally graded porous graphene reinforced nanocomposite plates based on a simple quasi-3D HSDT[J]. Thin-Walled Struct 2020;157:107151.
- [40] Motahare Masoumi, Mohsen Jahanshahi, Morteza Ghorbanzadeh Ahangari, Ghasem Najafpour Darzi. Electronic, mechanical and thermal properties of SiO₂ nanotube interacting with poly lactic-co-glycolic acid: Density functional theory and molecular dynamics studies. Applied Surface Science, Volume 546, 2021, 148894, ISSN 0169-4332, <https://doi.org/10.1016/j.apsusc.2020.148894>.
- [41] Zhaoxin Qiu, Zhibo Zhang, Yongnan Xiong, Xing Luo, Zhiqiang Li, Kaihong Zheng, Wangyu Hu, Size effects of graphene sheets on the strengthening mechanism of Al-graphene composites: A molecular dynamics study, Applied Surface Science, Volume 596, 2022, 153546, ISSN 0169-4332, <https://doi.org/10.1016/j.apsusc.2022.153546>.
- [42] Yishu Yan, Junbo Xu, Huajian Zhu, Yinxiang Xu, Min Wang, Bingyin Wang, Chao Yang, Molecular dynamics simulation of the interface properties of continuous carbon fiber/ polyimide composites, Applied Surface Science, Volume 563, 2021, 150370, ISSN 0169-4332, <https://doi.org/10.1016/j.apsusc.2021.150370>.
- [43] Huang Y, Lv M, Luo W, Zhang H, Geng D, Li Q. Sound Insulation Properties of Membrane-type Acoustic Metamaterials with Petal-like Split rings. J Phys D Appl Phys 2021;55:045104.
- [44] Li J, Shi Y, Jiang R, Zhang Z, Huang Q. Acoustic Insulation Mechanism of Membrane-Type Acoustic Metamaterials Loaded with Arbitrarily Shaped Mass Blocks of Variable Surface Density. Materials 2022;15(4):1556. <https://doi.org/10.3390/ma15041556>.
- [45] Langfeldt F, Gleine W, Estorff OV. An efficient analytical model for baffled, multi-celled membrane-type acoustic metamaterial panels. J Sound Vib 2018;417:359–75.
- [46] Zhifu Zhang, Zhuang Li, Tianyun Li, Qibai Huang, A novel semi-analytical approach for predicting the sound absorptions of a new underwater composite coating with transversely arranged SWCNTs, Composite Structures, Volume 274, 2021, 114335, ISSN 0263-8223, <https://doi.org/10.1016/j.comstruct.2021.114335>.
- [47] Naify CJ, Chang C-M, McKnight G, Nutt SR. Scaling of membrane-type locally resonant acoustic metamaterial arrays. J Acoust Soc Am 2012;132:2784–92.
- [48] Naify CJ, Chang C-M, McKnight G, Scheulen F, Nutt S. Membrane-type metamaterials: transmission loss of multi-celled arrays. J Appl Phys 2011;109:104902.
- [49] Saad Y. Numerical Methods for Large Eigenvalue Problems. 2nd ed. Philadelphia: Society for Industrial and Applied Mathematics; 2011.
- [50] Yuguang Zhang, Jihong Wen, Yong Xiao, Xisen Wen, Jianwei Wang, Theoretical investigation of the sound attenuation of membrane-type acoustic metamaterials, Physics Letters A, Volume 376, Issue 17, 2012, Pages 1489–1494, ISSN 0375-9601,

- [33] 叶飞, 陈飞, 方伟, 徐雷, 阮松, 刘晓, 钟明, 匡涛。高强度。
来源文本: 由热塑性聚氨酯和多壁碳纳米管制备的柔韧且循环稳定的压阻聚合泡沫 [J]。复合材料 B 部分: 工程, 已接受。
- [34] 费 Y, 方 W, 钟 M, 金 J, 范 P, 杨 J 等。挤出发泡
轻质聚苯乙烯复合泡沫具有可控的细胞结构, 用于吸声应用 [J]。聚合物 2019
年;11(1):106。
- [35] 方 W, 费 Y, 卢 H, 金 J, 钟 M, 范 P 等。增强隔音和
基于无机填料/热塑性弹性体复合材料的力学性能 [J]。J Thermoplast Compos Mater
2018;089270571876638。
- [36] 陈 S, 朱 W, 程 Y。聚氨酯泡沫复合材料声学性能的多目标优化。聚合物 2018
年;10(7):788。
<https://doi.org/10.3390/polym10070788>.
- [37] Albooyeh A, Dadrasi A, Mashhadzadeh AH. 点缺陷和低效果。
密度碳掺杂对 BNNTs 力学性能的影响: 一项分子动力学研究。材料化学物理学 2020
年; 239: 122107。
- [38] 徐志超, 黄 Q。功能梯度石墨烯的振动声学分析
在热机械载荷下加固的纳米复合层压板 [J]。Eng Struct 2019;186:345 - 55。
- [39] 徐志超, 张张, 王杰等。功能梯度声学分析
基于简单的准三维 HSDT 的多孔石墨烯增强纳米复合板。薄壁结构 2020
年;157:107151。
- [40] Motahare Masoumi, Mohsen Jahanshahi, Morteza Ghorbanzadeh Ahangari,
Ghasem Najafpour Darzi, SiO₂ 纳米管与聚乳酸-聚乙二醇酸相互作用的电子、机械
和热性质: 密度泛函理论和分子动力学研究, 应用表面科学, 第 546 卷, 2021 年,
148894, ISSN 0169-4332, <https://doi.org/10.1016/j.apsusc.2020.148894>。
- [41] 邱兆林, 张波, 熊永南, 罗兴, 李志强, 凯宏
郑, 王宇胡, 石墨烯片对 Al-石墨烯复合材料强化机制的尺寸效应: 分子动力学研
究, 应用表面科学, 卷 596, 2022 年, 153546, ISSN 0169-4332,
<https://doi.org/10.1016/j.apsusc.2022.153546>。
- [42] 言艺树, 徐俊波, 朱华健, 徐银祥, 王敏, 王炳银
超阳, 连续碳纤维/聚酰亚胺复合材料界面性能的分子动力学模拟, 应用表面科学,
第 563 卷, 2021 年, 150370, ISSN 0169-4332, <https://doi.org/10.1016/j.apsusc.2021.150370>.
- [43] 黄 Y, 吕 M, 罗 W, 张 H, 耿 D, 李 Q。声隔离性能
薄膜型声学超材料与花瓣状分裂环。J Phys D Appl Phys 2021;55:045104.
- [44] 李 J, 史 Y, 姜 R, 张 Z, 黄 Q。声学隔音机制
膜型声学超材料加载了表面密度可变的任意形状质量块。材料 2022
年;15(4):1556. <https://doi.org/10.3390/ma15041556>.
- [45] Langfeldt F, Gleine W, Estorff OV. 一个高效的受挡分析模型。
多孔膜型声学超材料面板。J Sound Vib 2018;417:359 - 75.
- [46] Zhifu Zhang, Zhuang Li, Tianyun Li, Qibai Huang, A novel semi-analytical
approach for predicting the sound absorptions of a new underwater
composite coating with transversely arranged SWCNTs, Composite Structures,
Volume 274, 2021, 114335, ISSN 0263-8223, <https://doi.org/10.1016/j.compstruct.2021.114335>.
- [47] Naify CJ, Chang C-M, McKnight G, Nutt SR. Scaling of membrane-type locally
resonant acoustic metamaterial arrays. J Acoust Soc Am 2012;132:2784 - 92. [48]
Naify CJ, Chang C-M, McKnight G, Scheulen F, Nutt S. Membrane-type
metamaterials: transmission loss of multi-celled arrays. J Appl Phys
2011;109:104902.
- [49] Saad Y. Numerical Methods for Large Eigenvalue Problems. 2nd ed.
Philadelphia: Society for Industrial and Applied Mathematics; 2011. [50]
Yuguang Zhang, Jihong Wen, Yong Xiao, Xisen Wen, Jianwei Wang, Theoretical
investigation of the sound attenuation of membrane-type acoustic
metamaterials, Physics Letters A, Volume 376, Issue 17, 2012, Pages
14891494, ISSN 0375-9601,